Special Session on Optical Properties of Atmospheric Aerosol — Observation, Measurement Techniques and Model Analysis for Improving the Accuracy of Aerosol Light Absorption Determinations in Polluted Sites (I)

Aerosol and Air Quality Research, 20: 663–679, 2020 Copyright © Taiwan Association for Aerosol Research

ISSN: 1680-8584 print / 2071-1409 online doi: 10.4209/aaqr.2019.06.0298



Comparison of Filter-based Absorption Measurements of Biomass Burning Aerosol and Background Aerosol at the Mt. Bachelor Observatory

James R. Laing¹, Daniel A. Jaffe^{1,2*}, Arthur J. Sedlacek, III³

- ¹University of Washington Bothell, Bothell, WA 98011, USA
- ² University of Washington, Seattle, WA 98195, USA
- ³ Brookhaven National Laboratory, Upton, NY 11973, USA

ABSTRACT

In this study we evaluate the recently upgraded aethalometer (AE33) and the newly released tricolor absorption photometer (TAP) with respect to their response to wildfire aerosol plumes during their deployment at the Mount Bachelor Observatory (MBO; 2763 m a.s.l.) in central Oregon, USA, during the summer of 2016. While both instruments use similar methodology (i.e., light extinction through an aerosol-laden filter), each has a unique set of correction schemes to address artifacts originating from filter loading, scattering from captured aerosol particles, and multiple scattering effects of the filter fibers. We also utilize a Single Particle Soot Photometer (SP2) to determine refractory black carbon (rBC) in these air masses. In addition to comparing the AE33 filter-loading correction methodology to previously published aethalometer correction schemes, we also compare the AE33 to the correction schemes used for the TAP and evaluate the degree to which the different correction factors influence the derived absorption Angström exponents (AAE) and mass absorption cross sections (MACs). We find that while the different correction factors for either the AE33 or TAP do exert an influence on the derived MACs, AAEs exhibit the most sensitivity to the correction schemes. Our study finds that using the AE33 manufacturer's recommended settings results in aerosol light absorption coefficients that are 3.4 to 4 times greater than the aerosol light absorption coefficients reported by the TAP. We calculated a correction factor (C_f) of 4.35 for the AE33 by normalizing the AE33 to match the TAP. The uncorrected AE33 also gives equivalent black carbon (eBC) values that are approximately 2 times the rBC measured by the SP2 instrument. We also find that biomass burning aerosols result in significant MAC enhancements, particularly at lower wavelengths, which is attributable to brown carbon (BrC).

Keywords: Aerosol scattering; Aerosol absorption; SP2; AE33; TAP; PSAP.

INTRODUCTION

Aerosols play an important role in the Earth's radiative budget by directly scattering and absorbing solar radiation (Myhre *et al.*, 2013). Light absorption by aerosols is dominated by carbon species emitted during the combustion of biomass or fossil fuels. While the most important light-absorbing aerosol remains black carbon (BC) (Bond *et al.*, 2006, 2013) it is now recognized that brown carbon (BrC) is also important. These light-absorbing organic aerosols are emitted primarily in biomass burning (BB) and are distinguished by their preference to absorb at near-UV wavelengths (Kirchstetter *et al.*, 2004; Andreae and Gelencser, 2006; Saleh *et al.*, 2013). Given the increase in wildfire activity (Dennison *et al.*, 2014; Abatzoglou and Williams, 2016) and the large aerosol mass that these events inject into the atmosphere, having accurate measurements of

aerosol absorption by BB aerosols is crucial for improved quantification of the contribution to aerosol radiative forcing.

Measurement of light absorption using a filter-based instrument, which is the predominate method used in the field, derive the absorption coefficient, σ_{abs} , by measuring the change in light attenuation due to aerosol loading on a filter (Hansen et al., 1984; Bond et al., 1999). The raw attenuation (ATN) coefficient (σ_{ATN} , Mm⁻¹) can be thought of as the uncorrected absorption coefficient as it contains contributions from both light absorption and scattering from both the captured aerosol particles on the filter and the filter media itself. To derive the desired light absorption coefficients, σ_{ATN} must be corrected for measurement artifacts unique to this class of instrumentation and include contributions from the filter itself and potential modification of aerosol optical properties due to the deposition of these particles onto the filter. These measurement corrections fall into three major classes: (1) filter-loading corrections, which correct for the accumulation of light-absorbing particles on the filter that reduce the optical path; (2) multiple light-scattering corrections, which correct incident light scattered by the filter fibers of

^{*} Corresponding author. E-mail address: djaffe@uw.edu

an unloaded filter; and (3) aerosol scattering corrections, which correct for the incident light scattered off of light-scattering particles loaded onto the filter (Bond et al., 1999). These artifacts limit the accuracy of these measurements to 20-30% (Springston and Sedlacek III, 2007; Bond et al., 2013). Another subtle, but important, consideration is that upon contact with the filter the aerosol particle morphology could be altered leading to further uncertainty, which is not captured by corrections currently used. Still further complications can be encountered when liquid-like organic aerosols (OA) coat the filter fibers (Subramanian et al., 2007) or interact with the probe light leading to enhanced absorption (Lack et al., 2008). Indeed, when the ratio of OA to BC is high, as is common for biomass burn events, filter-based absorption coefficients have been shown to be biased high by 50–80% (Cappa et al., 2008; Lack et al., 2008; Kondo et al., 2009). In-situ measurement of aerosol absorption instruments using photoacoustic spectroscopy (PAS) or photothermal interferometry (PTI) have less biases and lower uncertainties compared to filter-based instruments (Moosmuller et al., 2009; Bond et al., 2013), but these methods are more complex and require more care during operation.

The lower cost and minimal maintenance of filter-based instruments has made them preferred for long-term observations of aerosol light absorption. The National Oceanic and Atmospheric Administration (NOAA), the Global Atmosphere Watch (GAW) program, and the U.S. Department of Energy's Atmospheric Radiation Measurement (ARM) program have used various filter-based instruments to measure aerosol light absorption at their long-term surface research sites since the 1990s and will continue to use these instruments into the future (Ogren *et al.*, 2017; Andrews *et al.*, 2019).

In this study we evaluate the response of two filter-based instruments with respect to wildfire plumes where filterbased bias in these measurements is expected to be highest: the tricolor absorption photometer (TAP, Brechtel Inc., Hayward, CA) and the recently updated aethalometer (model AE33, Magee Scientific, Berkeley, CA). The TAP measures absorption coefficients at 465, 520, and 640 nm, while the AE33 measures absorption coefficients at 370, 470, 520, 590, 660, 880, and 950 nm. Motivation for conducting absorption measurements at multiple wavelengths is that it allows for the quantification of the wavelength dependence, which can be used to distinguish between BC and BrC—the latter being light-absorbing organic aerosols. Given the likely continued and future use of the TAP and AE33, it is imperative to characterize these two instruments for a range of conditions so that absorption measurements derived from these instruments can be harmonized and compared.

Our goals for this study are:

- 1. Evaluate the efficacy of TAP and AE33 filter-loading and scattering correction schemes for wildfire aerosols.
- 2. Examine if the derived absorption Ångström exponents (AAEs) from the TAP and AE33 exhibit a dependence on correction methods and, if a dependence is found, evaluate the extent to which this dependence influences apportionment of BC and BrC absorption via AAE.
- 3. Derive and compare mass absorption cross sections

(MACs) for the TAP and AE33 using refractory black carbon (rBC) mass concentrations reported by a co-located Single Particle Soot Photometer (SP2).

METHODS

Mt. Bachelor Observatory

The Mount Bachelor Observatory (MBO), located at the summit of Mt. Bachelor in central Oregon, USA (43.98°N, 121.69°W, 2764 m a.s.l.), is a mountaintop site that has been in operation since 2004 (Jaffe et al., 2005). A suite of measurements (including carbon monoxide (CO), ozone (O₃), aerosol scattering coefficients, and metrological measurements) have been made continuously at the summit site since measurements began. This unique location has allowed the study of BB plumes in the free troposphere from regional and distant sources in the spring, summer, and fall (Weiss-Penzias et al., 2007; Wigder et al., 2013; Timonen et al., 2014; Baylon et al., 2015; Briggs et al., 2016; Collier et al., 2016; Zhou et al., 2017), and long-range transport of Asian pollution in the spring (Jaffe et al., 2005; Weiss-Penzias et al., 2006; Fischer et al., 2010a, b; Reidmiller et al., 2010; Ambrose et al., 2011; Timonen et al., 2013, 2014; Gratz et al., 2015; Zhang and Jaffe, 2017).

At MBO the instruments are located in a temperature-controlled room within the summit building, situated approximately 15 m below the aerosol inlet. The aerosol sample line is designed so that the last 2.5 m is located within a space that is temperature controlled at ~20°C. All measurements were downstream of a PM $_{\rm l}$ cut size impactor. When outside relative humidity (RH) is high (> 50%), the temperature difference between the outside and instrument room reduces the RH of the sample airstream. During the campaign the RH measured by the nephelometer was < 35%. The measurements discussed here range from July through September 2016.

Tricolor Absorption Photometer (TAP)

Aerosol light absorption coefficients (σ_{absTAP}) were also measured with a 3-wavelength (λ) tricolor absorption photometer (TAP, Brechtel Inc., Hayward, CA) at wavelengths 465, 520, and 640 nm. We used quartz filters (Pallflex, E70-2075W) throughout the campaign. The TAP is the commercially available version of NOAA's continuous light absorption photometer (CLAP) (Ogren *et al.*, 2017). From a measurement methodology point of view, the CLAP and TAP are similar to the Particle Soot Absorption Photometer (PSAP), except for the feature of being able to sample sequentially through eight spots on a single filter thereby allowing these two instruments to operate 8x longer before requiring a technician to replace the filter media. A detailed description of the CLAP is provided in Ogren *et al.* (2017).

For this study, we set the transmittance threshold whereupon the TAP starts collecting sample on a new spot at 0.7 to minimize loading effects and complications arising from the departure from signal linearity—this translates to an ATN of 36. The reported TAP σ_{abs} were flow and spot size corrected. One distinguishing hardware attribute between the CLAP

and the TAP is that the latter uses O-rings to create a seal between the filter holder and the filter itself. Securing the filter this way leads to more ambiguous edges in the actual spot area and impacts the derived absorption cross section. Due to the ambiguity in the edge of the filter spot we used the manufacturer's recommended value of (30.721 mm^2) and estimate the uncertainty in spot area to be $\sim 20\%$.

The two correction methods for the TAP used in this study come from (1) Ogren (2010), which updated the Bond *et al.* (1999) correction, (2) and Virkkula *et al.* (2005), which was updated by Virkkula (2010). Both correction algorithms were developed empirically and correct for aerosol loading and apparent absorption from light-scattering particles. The Bond *et al.* (1999) correction was developed for the 1 λ PSAP (567 nm) and updated for the 3 λ PSAP in Ogren (2010), whereas the Virkkula (2010) correction was developed for the 3 λ . The details for these corrections are in Table S1. We did not evaluate the Müller correction method (Müller *et al.*, 2014), which uses a two-stream radiative model, but is complicated to implement.

Aethalometer (AE33)

A newly upgraded 7-wavelength aethalometer model AE33 (Magee Scientific, Berkeley, CA) was used to measure light absorption coefficients (σ_{absAE}) at wavelengths of 370, 470, 520, 590, 660, 880, and 950 nm (Drinovec *et al.*, 2015). Like with the TAP, we set the criteria for using a new filter spot at a light ATN threshold of 120, which translates to a transmittance of 0.36. This threshold is very low and puts the optical measurement in the non-linear condition, so in post-processing we removed data with transmittance < 0.5. As mentioned above, the AE33 is an upgraded model of the aethalometer in that offers a real-time aerosol-loading compensation algorithm using DualSpotTM technology (Drinovec et al., 2015). Specifically, the AE33 uses two spot measurements with different flow rates and, thus, different aerosol-loading rates. By using these two measurements, a reduction in the bias on aerosol loading by filter loading can be realized. This allows for the calculation of real-time filterloading correction. Henceforth, this dual-spot filter-loading correction, k_D, is referred to as the Drinovec correction.

The AE33 outputs equivalent black carbon (eBC) mass concentrations. Black carbon is operationally defined and Petzold *et al.* (2013) suggested "BC" concentrations derived from absorption measurements should be called equivalent black carbon. Absorption coefficients ($\sigma_{absAE33}$) were "back-calculated" from the reported eBC values using the AE33 mass absorption cross sections (MAC_{AE33}) used internally by the instrument.

$$\sigma_{absAE33-Drinovec} = eBC \times MAC_{AE33} \tag{1}$$

the MAC_{AE33} values are 18.47, 14.54, 13.14, 11.58, 10.35, 7.77, and 7.19 m² g⁻¹ for 370, 470, 520, 590, 660, 880, and 950 nm, respectively (Drinovec *et al.*, 2015). Attenuation coefficients (σ_{ATN}) were obtained by removing the Drinovec filter-loading correction ($1 - k_D \times ATN$) and the multiple scattering correction, C_{ref} (which were automatically applied to the aethalometer output).

$$\sigma_{ATN} = \sigma_{absAE33-Drinovec} \times (1 - k_D \times ATN) \times C_{ref}$$
 (2)

the σ_{ATN} determined in Eq. (2) is used as the base to explore other filter-loading corrections.

Two differences between the AE33 and previous versions of the aethalometer (e.g., AE31) are the filter media and MAC values used internally to calculate eBC mass concentrations. The upgraded AE33 uses a tetrafluoroethylene (TFE)-coated glass fiber filter tape, whereas the older version aethalometers use a quartz fiber filter tape. The TFE-coated glass fiber filter tape is less sensitive to air sample relative humidity. The aethalometer MACs are empirically derived and the AE31 MAC values are more than twice as large as the AE33 MAC values. This means that although the AE31 and AE33 eBC mass concentrations show good correlation (slopes from 0.9 to 1.19) (Drinovec *et al.*, 2015; Rajesh and Ramachandran, 2018), the derived σ_{abs} reported by the AE31 are expected to be much higher.

There are various post-processing correction schemes for aethalometers to address for filter-loading, scattering effects of loaded aerosol, and multiple scattering effects of the filter (Weingartner *et al.*, 2003; Arnott *et al.*, 2005; Schmid *et al.*, 2006; Virkkula *et al.*, 2007; Collaud Coen *et al.*, 2010). Some studies have combined parts of different correction schemes together, making direct comparisons difficult (Yang *et al.*, 2009; Segura *et al.*, 2014; Ran *et al.*, 2016; Segura *et al.*, 2016; Wang *et al.*, 2017).

Collaud Coen *et al.* (2010) evaluated AE31 correction algorithms and proposed a new correction algorithm based on data collected from four European sites with several types of aerosols (free tropospheric, urban, maritime, and rural background). They included four filter-loading corrections (Arnott, Virkkula, Weingartner, and Collaud Coen) and two scattering corrections (Arnott and Schmid). They also presented a new scattering correction parameterization that essentially creates two new scattering corrections, using the same Arnott and Schmid equations but using different parameter values. Saturno *et al.* (2017) differentiates between these as the "Arnott" correction and the "Collaud Coen's Arnott-like" correction. In our study we refer to the Arnott and Schmid scattering corrections using Collaud Coen's nomenclature as Arnott-b and Schmid-b, respectively.

In this paper we will evaluate a subset of the filter-loading and scattering corrections detailed in Collaud Coen et al. (2010) in comparison with the dual-spot Drinovec correction for aerosols produced in biomass burning. We do not implement the Arnott filter-loading correction (Arnott et al., 2005) as it was deemed in Collaud Coen et al. (2010) to produce a significant number of outliers and exhibited the highest standard deviation when compared to Multiangle Absorption Photometer (MAAP) data. In summary, the filterloading corrections evaluated are the Drinovec, Virkkula, Weingartner, and Collaud Coen correction algorithms. We also examine the scattering corrections to the Drinovec filter-loading correction so as to evaluate their effect. The scattering corrections evaluated are the Arnott, Schmid, Arnott-b, and Schmid-b scattering corrections. The details for the corrections are in Table S1.

Single Particle Soot Photometer (SP2)

Refractory BC (rBC) mass concentration was measured using a Single Particle Soot Photometer (SP2; Droplet Measurement Technologies, Longmont, CO). To differentiate from other BC concentrations, Petzold et al. (2013) suggested "BC" concentrations from laser-induced incandescence report their concentrations as refractory black carbon. Detailed SP2 operating principles and analysis procedures have been previously described and thus will only be highlighted here (Stephens et al., 2003; Schwarz et al., 2006; Moteki and Kondo, 2007; Schwarz et al., 2008b; Moteki and Kondo, 2010). In brief, the SP2 measures the time-dependent scattering and incandescence signals generated by individual BCcontaining particles as they travel through a continuouswave laser beam operating at 1064 nm. If the interrogated particle contains a BC component, some of the laser energy will be absorbed until the temperature of the BC component is raised to the point of incandescence. The individual particle incandescence signals are converted to particle mass (obtained via calibration) that can then be converted to an equivalent diameter to yield a BC-specific size/mass distribution. In keeping with the nomenclature advocated by the SP2 community, we henceforth refer to the incandescence BC component as refractory black carbon (rBC). During the deployment at MBO, the SP2 detected incandescence signals from particles with a mass equivalent diameter in the range of 60-400 nm. We calibrated the SP2 scattering channel using size-selected polystyrene latex spheres (PSL) and the incandescence channel using fullerene soot (Alfa Aesar; stock no. 40971; lot no. L18U002) prior to and after the campaign. Uncertainties in BC mass concentration are estimated to be $\pm 30\%$.

Additional Measurements and Calculations

Aerosol light-scattering coefficients (σ_{scat}) were measured using an integrating nephelometer (model 3563, TSI, Inc., Shoreview, MN) at wavelengths 450, 550, and 700 nm. The σ_{scat} values were corrected for drift and scattering truncation according to the scheme laid out by Anderson and Ogren (1998). Dry particle aerosol number size distribution was measured with a Scanning Mobility Particle Sizer (SMPS; model 3938, TSI, Inc., Shoreview, MN). Details regarding calibrations and corrections are available in Laing *et al.* (2016).

Comparison of the derived AAE values for the TAP and AE33 were calculated using σ_{abs} measured at wavelengths (λ) 470 and 660 nm using Eq. (3). Single scattering albedo (SSA) values used throughout the study were calculated with Eq. (4) at 520 nm.

$$AAE = -\frac{\log(\sigma_{abs}(\lambda_1)/\sigma_{abs}(\lambda_2))}{\log(\lambda_1/\lambda_2)}$$
(3)

$$SSA = -\frac{\sigma_{scatTAP}}{\sigma_{scat} + \sigma_{absTAP}} \tag{4}$$

The TAP measures aerosol light absorption at different

wavelengths than the AE33. Therefore, to facilitate direct comparison between the two instruments, the derived absorption coefficients from the TAP (σ_{absTAP}) were interpolated from 465 nm to 470 nm, and from 640 nm to 660 nm, the wavelengths of the AE33, using the equation below.

$$\sigma_{abs}(\lambda_1) = \sigma_{abs}(\lambda_2)[\lambda_2/\lambda_1]^{AAE}$$
(5)

The TAP wavelength-adjusted σ_{abs} at 470 nm was derived from the TAP σ_{abs} at its native wavelength of 465 nm using AAE values calculated for the 465–520 nm wavelength pair. Similarly, the TAP wavelength-adjusted σ_{abs} at 660 nm used the σ_{abs} at 640 nm and AAE values for the 520–640 nm pair. These AAE values are just used to interpolate the σ_{abs} , and not used throughout the rest of the manuscript.

All particle measurements were corrected to standard temperature and pressure (STP; T = 273.15, P = 101.325 kPa).

RESULTS AND DISCUSSION

The campaign was separated into BB-influenced periods and nonBB periods. During the campaign the MBO site was engulfed by three days of wildfire smoke (Fig. 1; 8/29/2016 to 9/1/2016) from the Gap Fire, in northern California. Transport time from the fire origin to MBO is estimated to range from 10 to 15 hours using HYSPLIT back-trajectories.

BB periods were defined as any 5-min average with aerosol scattering at (550 nm) > 15 Mm⁻¹ during the Gap Fire. During the BB periods the $\Delta\sigma_{scat}/\Delta CO$ was 0.84 (R² = 0.90), very consistent with previous BB events at MBO (Laing *et al.*, 2016). All other periods are assumed to be nonBB periods and thus represent regional background air masses. Using monthly water vapor criterion developed by (Zhang and Jaffe, 2017) to distinguish between free troposphere (FT) and boundary layer–influenced (BLI) air masses, we find that 66% of the nonBB period were FT and 34% were BLI.

Intra-comparison of Filter-based Absorption Correction Methods

TAP Corrections

The TAP absorption coefficients were corrected using the algorithms developed by Ogren (2010) and Virkkula (2010), hereby referred to as O2010 and V2010, respectively. Compared to just the O2010 and V2010 filter-loading corrections, adding the scattering corrections decreases the derived σ_{absTAP} by 20–36% (Fig. S1). This decrease is large due to the high SSA values, indicating a large scattering component of the aerosol throughout the campaign (between 0.9 and 1). The scattering corrections are a fraction of σ_{scat} subtracted from the σ_{abs} so the greater the SSA, the greater the impact of the scattering correction.

The O2010 correction is the updated Bond *et al.* (1999) correction, where the correction schemes were extended beyond the single-wavelength PSAP instrument (567 nm) used by Bond. The reference instruments used to develop the Bond *et al.* (1999) correction measured at 550 nm, thus the corrected absorption value was reported at 550 nm. The O2010 correction expanded the Bond *et al.* (1999) correction

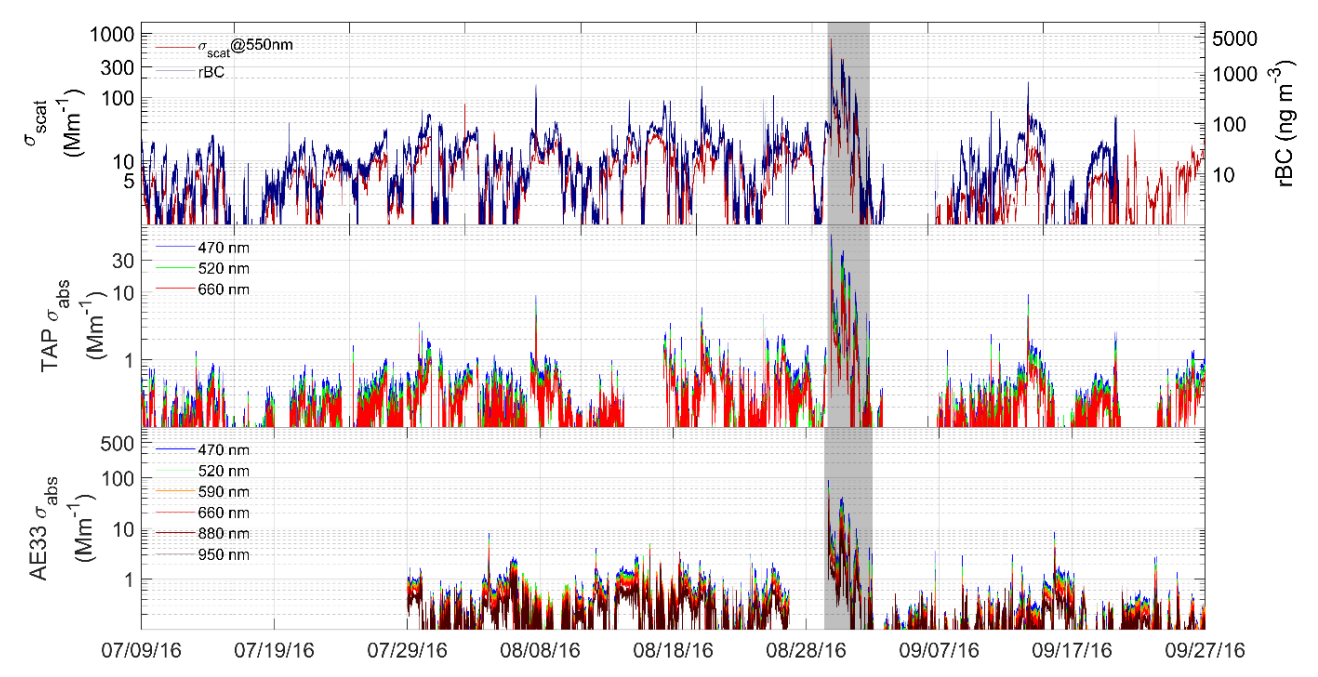


Fig. 1. Time series of 5-min averaged data during the 2016 summer campaign. The designated BB period is shaded.

to remove the implicit adjustment to 550 nm and provide corrections for three-wavelength PSAPs. The O2010 correction parameters are the same for every wavelength, whereas the V2010 corrections were developed for the three-wavelength PSAP and thus have wavelength-specific correction parameters (Table S1). One direct consequence of this is that the correction schemes for V2010 and O2010 σ_{absTAP} are inconsistent across wavelengths (Fig. 2). For example, at 470 nm the slope between V2010 and O2010 is 1.06, whereas at 660 nm the slope is 0.83. As discussed later in "Comparison of AAEs" section, these differences have strong implications for derived AAE values and the subsequent compositional interpretation of the sampled aerosol when using AAE values.

AE33 Corrections

Filter-loading Corrections

In this section we first compare the performance of the Drinovec filter-loading correction with previously published aethalometer filter-loading corrections and then extend this evaluation to assess the impact of scattering corrections with the Drinovec filter-loading correction. To this end we evaluated three filter-loading corrections (Virkkula (R_V) (Virkkula *et al.*, 2007), Weingartner (R_W) (Weingartner *et al.*, 2003), and Collaud Coen (R_C) corrections (Collaud Coen *et al.*, 2010)) against the new dual-spot Drinovec correction (R_D). These correction schemes are defined in Table S1.

The Virkkula correction employs a parameter (k_i) that aligns the last measurement on a filter spot with the first measurement on the next filter spot. Determining the Virkkula k_i values proved challenging due to the high variability of absorption coefficients between filter changes, especially during the biomass burning periods. The k_i values were calculated as described in Virkkula *et al.* (2007), but minimum and maximum values of -0.005 and 0.010 were set such that calculated k_i values that fell outside theses limits were set to

either the minimum or maximum allowable threshold value. The chosen minimum and maximum limits span the range observed in Virkkula *et al.* (2007). Most of the filter spots end up with a Virkkula k_i value of 0.010, which is a typical value for wood smoke (Allen *et al.*, 2011).

The derived Virkkula σ_{absAE} have similar values to the Drinovec σ_{absAE} across all wavelengths with slopes increasing with wavelength from 0.96 at 370 nm to 1.05 at 950 nm (Fig. S2). The Weingartner σ_{absAE} and Collaud Coen σ_{absAE} agree well with Drinovec σ_{absAE} at high wavelengths, but the slope decreases with decreasing wavelength. This is likely due to the wavelength dependence of the Drinovec correction factor.

The Drinovec correction (R_D) shows a clear wavelength dependence. This wavelength dependence was observed for the Virkkula correction (R_V) when the Virkkula k_i values are positive. Due to high aerosol SSA (0.9–1) throughout the campaign, the Weingartner (R_W) and Collaud Coen correction factors (R_C) stayed near unity at all wavelengths. For both Weingartner and Collaud Coen, as SSA approaches 1, R_W and R_C approach 1. The wavelength dependence of the derived AAEs on the correction schemes will be discussed in "Comparison of AAEs" section.

Scattering Corrections

We evaluated four scattering corrections, (1) Arnott (Arnott *et al.*, 2005), (2) Schmid (Schmid *et al.*, 2006), (3) Arnottb, and (4) Schmid-b (Collaud Coen *et al.*, 2010). The Arnott and Schmid correction schemes use scattering correction parameters $\alpha(\lambda)$ as defined in Arnott *et al.* (2005). Collaud Coen *et al.* (2010) updated the Arnott and Schmid scattering correction schemes by creating new parameter values $\alpha(\lambda)$; and by using the mean σ_{absAE} and SSA since the last filter spot change instead of the σ_{absAE} and SSA measured simultaneously at the time of the absorption measurement. The updated

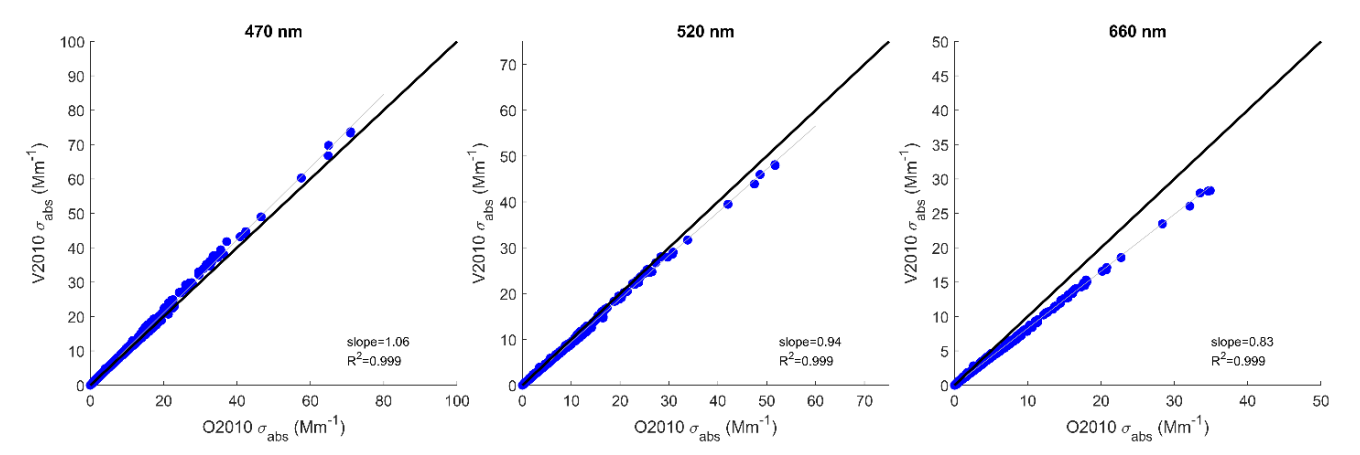


Fig. 2. Comparison of σ_{absTAP} calculated using V2010 and O2010 correction schemes using 5-min averages. The solid line is 1:1.

versions of the Arnott and Schmid scattering correction schemes are Arnott-b and Schmid-b, respectively. All four of these scattering correction schemes are defined in Table S1 and further detailed in Collaud Coen *et al.* (2010).

To evaluate the scattering corrections, we added them to the Drinovec filter-loading corrected σ_{absAE} . For both scattering corrections, using the Arnott values decreases σ_{absAE} significantly more than using the Collaud Coen values (Figs. S3 and S4). The Arnott scattering correction with Arnott parameter values decreases σ_{absAE} the most (from 13–33%, increasing with wavelength), and the Schmid scattering correction with Arnott parameter values decreases σ_{absAE} the second most (~18%). Using the Collaud Coen parameter values in the Arnott scattering correction decreases the σ_{absAE} by ~5% and using the Collaud Coen parameter values in the Schmid scattering correction decreases the σ_{absAE} by 5–8%, which decreases with wavelength.

Multiple Scattering Correction

The multiple scattering correction (C_{ref}), which addresses the scattering effects of the filter itself, is the most variable of the three corrections available for aethalometer-derived σ_{abs} values. This variability in C_{ref} for the AE33 represents a major source of uncertainty.

The C_{ref} for Pallflex Teflon-coated glass fiber (TFE) filter tape is set to 1.57 in the AE33 software and is not wavelength dependent (Drinovec et al., 2015). This manufacturer's default C_{ref} of 1.57 is based on a 2-week campaign involving two collocated AE33s—one with TFE tape and the other with quartz filter tape. A C_{ref} of 2.14 was assumed for the quartz filter as per Weingartner et al. (2003), and Cref of 1.57 for the TFE filter was obtained by setting the BC values at ATN = 0 equal for both filters. The C_{ref} value of 2.14 is based on laboratory-generated fresh soot particles and diesel particles mixed with ammonium sulfate (Weingartner et al., 2003). Ambient measurements using aethalometers with glass fiber tape have reported C_{ref} values from 3 to 8, and have shown C_{ref} to depend on location, season, and aerosol type (Collaud Coen et al., 2010; Laborde et al., 2013; Segura et al., 2014; Segura et al., 2016; Backman et al., 2017; Saturno et al., 2017). This suggests the "default" value of 2.14 is too low. Indeed,

Müller (2015) recommended a wavelength-independent C_{ref} value for the AE31 of 3.5 ± 0.875 based on data from eight European monitoring stations. Similar values (e.g., ~3.5) were reported by Segura *et al.* (2016) and Zanatta *et al.* (2016). Müller (2015) also recommended a wavelength-independent C_{ref} for the AE33 of 3.2 based on measurements in Leipzig but stated that more data was needed for a more comprehensive evaluation.

Ideally, calculation of the multiple-scattering correction factor should require a collocated reference absorption instrument such as a MAAP (Weingartner *et al.*, 2003) or one of the in-situ techniques (e.g., PAS or PTI). Absent such a reference measurement, we are left with having to choose which dataset will serve as our benchmark. A recent study has shown the TAP σ_{abs} to be within \pm 30% of in-situ σ_{abs} measured using PAS for fresh and aged BB aerosol (Davies *et al.*, 2019). Since this is near the accuracy of filter-based absorption instruments, we can justify using the TAP as the reference absorption method to harmonize the AE33 σ_{abs} . As the TAP is also a filter-based absorption instrument that exhibits similar biases as the AE33, we calculate a correction factor (C_f) instead of a C_{ref} , which we define here as,

$$C_f = \sigma_{ATN AE33} / \sigma_{absTAP} \tag{6}$$

This approach was recently utilized by Backman *et al.* (2017) to harmonize aethalometer σ_{abs} with σ_{abs} from other filtered-based instruments (PSAP, CLAP, and MAAP) at six Arctic stations and where they recommend a C_f value of 3.45. Kim *et al.* (2018) calculated C_{ref} values of between 4.27 and 5.01 using a Photoacoustic Soot Spectrometer (PASS-3; Droplet Measurement Technologies, Inc., Longmont, CO), and when they applied these to aethalometer σ_{abs} measured at GSN (Gosan, Korea), LLN (Lulin, Taiwan), and ALT (Alert, Canada) stations found the difference to be ~9% compared to CLAP σ_{abs} . We must emphasize that we are not suggesting the TAP is a better instrument than the AE33 or that the AE33 absorption coefficients are "wrong", but rather that this approach allows us to harmonize the TAP and AE33 σ_{abs} data.

The correction factors, C_fs, were derived using all (BB and nonBB) 5-min data points at 470, 520, and 660 nm

(Table 1). The C_fs used V2010 corrected σ_{absTAP} values and the 5-min averaged data were filtered to exclude values of σ_{absTAP} and σ_{absAE} that were less than the method detection limit (MDL)— which was set as three times the standard deviation of 5-min averaged σ_{absTAP} while sampling HEPAfiltered air. The C_f values for the BB period are significantly lower than the nonBB periods at 470 nm. There is an inversely proportional relationship between C_f and AAE at 470 nm, which is slightly seen at 520 nm, and not observed at 660 nm (Fig. S5). Another noteworthy trend was also found between C_f and SSA (Fig. S6). At all wavelengths, C_f ranges from 3-6 from SSA 0.9 to 0.95. From SSA 0.95 to 0.98, C_{f470nm} and C_{f520nm} increase exponentially. C_f values have a slight downward trend with increasing aethalometer ATN, which is expected due to filter loading (Fig. S7). C_f values for all three wavelengths are highest when SSA is high (> 0.95) and AAE is equal or below 1 (Fig. S8). We further investigate the role of compositional dependence on Cf using an aerosol classification scheme using the AAE and scattering Ångström exponent (SAE) relationship (Cappa et al., 2016). According to this classification scheme, large C_f values (> 5) are associated with small, BC-dominated particles (Fig. 3), whereas C_f values < 5 are not defined by an individual sector and, instead, represent aerosols consisting of BrC. The C_f trends with AAE and SSA are not ATN dependent as they are observed even when only σ_{ATN} values with ATN < 10% are used.

For the remainder of the manuscript the mean value for C_f = 4.35 derived at 470, 520, and 660 nm is used to correct σ_{absAE} at all wavelengths for AE33 data.

Inter-comparison of Filter-based Absorption Coefficients (TAP and AE33 σ_{abs})

Absorption Coefficients

In this section we compare the V2010-corrected σ_{absTAP} values to σ_{absAE} values corrected using the methods discussed above. The filter spot changes were not synchronized between the AE33 and TAP, meaning the TAP filter spot changes and AE33 filter spot changes did not occur at the same time. This means the filter-loading effects based on transmittance (or attenuation) were not uniform for the TAP and AE33 throughout the campaign.

While the regression slopes between σ_{absTAP} and σ_{absAE} range from 0.79 to 1.11 for all aethalometer correction methods (Figs. S9–S12), it is important to remember that C_f essentially forces σ_{absAE} to agree with σ_{absTAP} and thus these

Table 1. Aethalometer C_f for all data points, BB periods, and nonBB periods at 470, 520, and 660 nm. The values were calculated as the mean C_f for the designated time periods when $\sigma_{abs} > MDL$.

Data selection			Correction factor	(C_f)
Data selection	П	470 nm	520 nm	660 nm
All data	4844	4.35 ± 2.04	4.45 ± 1.78	4.24 ± 1.86
BB periods	544	3.60 ± 0.81	4.04 ± 0.79	4.31 ± 0.77
NonBB periods	4134	4.50 ± 2.11	4.55 ± 1.87	4.28 ± 1.95

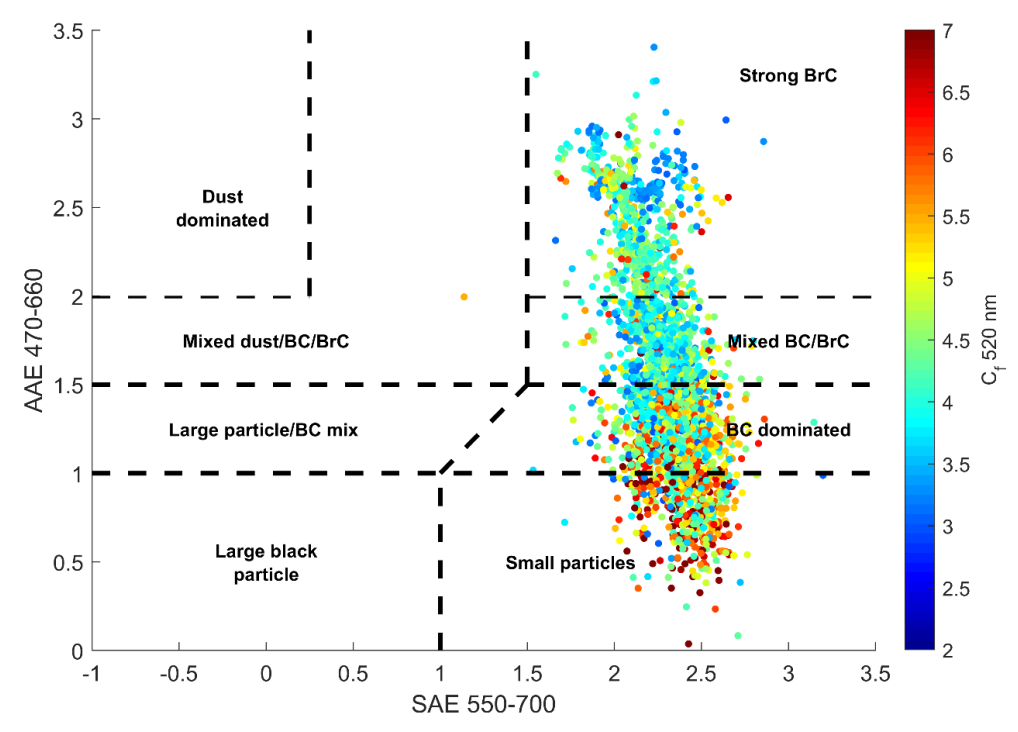


Fig. 3. Scatter plot of AAE (470–600 nm) and the SAE (550–650 nm pair) colored by aethalometer correction factors (C_f) for 520 nm and the aerosol classification index suggested by Cappa *et al.* (2016).

slopes cannot be taken as an indicator of which correction method is best. Using all 5-min averages, the reduced major axis (RMA) regression fit between σ_{atnAE} and σ_{absTAP} was similar for all aethalometer correction methods (R² ranged from 0.957 to 0.984; Figs. S9–S12).

The ratio $\sigma_{absAE\text{-corrected}}/\sigma_{absTAP}$ was compared to AAE and exhibited a general decreasing trend with increasing AAE values at 470 and 520 nm for all filter-loading and scattering corrected σ_{absAE} (Fig. 4). At 660 nm the $\sigma_{absAE\text{-corrected}}/\sigma_{absTAP}$ exhibited no trend with AAE. This indicates that either the AE33 underestimates (or the TAP overestimates) BrC absorption, which preferentially absorbs at shorter wavelengths. It has been shown that the PSAP can overestimate absorption at low wavelengths due to the beading of liquidlike BB organic aerosol onto filter fibers (Subramanian et al., 2007; Cappa et al., 2008; Lack et al., 2008; Lack et al., 2012). It is possible this mechanism and subsequent absorption enhancement at lower wavelengths varies depending on the filter materials (TAP used quartz filter; AE33 used Tefloncoated glass fiber filters) or different flow rates (TAP-1 LPM; AE33—2.5 LPM). Different flow rates and, therefore, filter face velocity influence absorption measurements by

changing the particle penetration depth into the filter (Moteki *et al.*, 2010; Nakayama *et al.*, 2010).

A dramatic increase in $\sigma_{absAE-corrected}/\sigma_{absTAP}$ is observed with an increase in SSA (Fig. 5). This increase is seen at all wavelengths and all AE33 correction methods but is least exaggerated when the Arnott and Schmid scattering corrections (with Arnott parameter values) are employed. Müller *et al.* (2014) showed that σ_{abs} measured with a PSAP and corrected with V2010 were 1.1 to 1.3 times higher than reference σ_{abs} for SSA > 0.9. Given this, the high $\sigma_{absAE-corrected}/\sigma_{absTAP}$ values are most likely due to the AE33 σ_{abs} not accurately correcting for highly scattering aerosol.

Comparison of SSAs

The SSA values (520 nm) throughout the campaign were very high with 95% of SSA values between 0.90 and 0.98. These values are similar to previous measurements at 532–550 nm of aged BB plumes (0.94 to 0.98 during BORTAS-B (Taylor *et al.*, 2014); 0.91 to 0.97 at MBO (Briggs *et al.*, 2016); 0.967 \pm 0.022 during ARCPAC (Brock *et al.*, 2011)). As the SSA is dominated by scattering, the agreement of the derived SSAs for the different TAP and AE33 correction

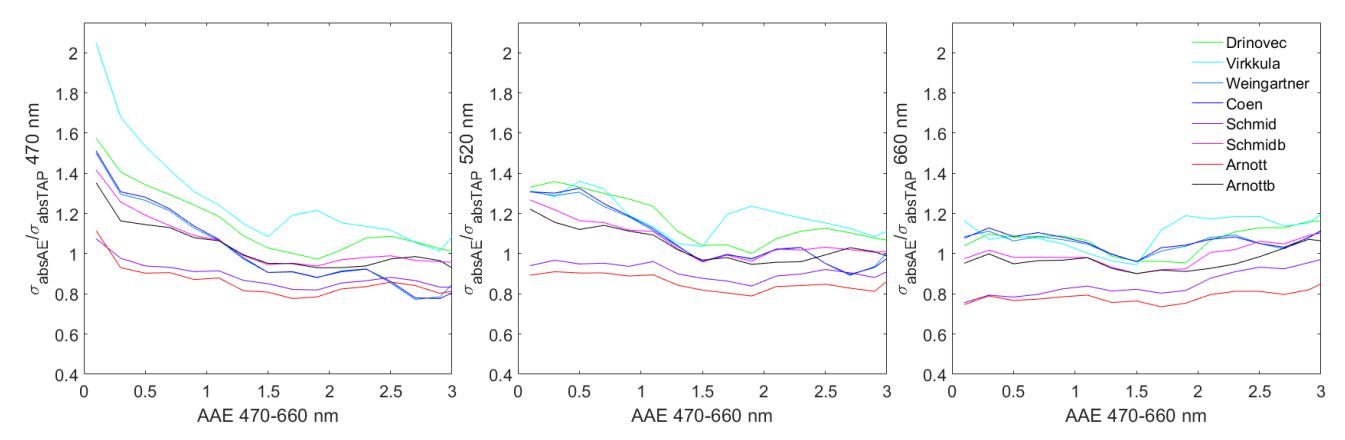


Fig. 4. $\sigma_{absAE}/\sigma_{absTAP}$ at 470, 520, and 660 nm as a function of TAP AAE calculated for the 470–660 nm wavelength pair for Drinovec, Virkkula, Weingartner, Coen, Arnott, Arnott-b, Schmid, and Schmid-b correction methods. The TAP AAE values were calculated using the V2010 corrected σ_{absTAP} .

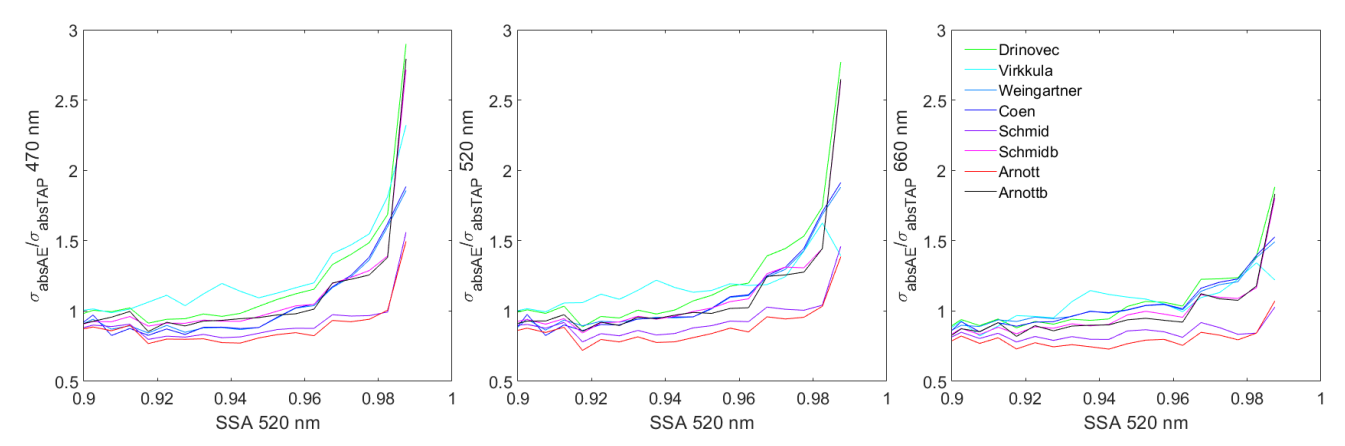


Fig. 5. $\sigma_{absAE}/\sigma_{absTAP}$ at 470, 520, and 660 nm as a function of SSA for Drinovec, Virkkula, Weingartner, Coen, Arnott, Arnott-b, Schmid, and Schmid-b correction methods. The SSA values were calculated using V2010 corrected σ_{absTAP} at 520 nm.

methods is not surprising as light absorption is relatively modest. The campaign median SSA values for all TAP and AE33 correction methods ranged from 0.942 to 0.955 (Table S2).

Comparison of AAEs

Eq. (3) was used to calculate AAE values for the 470 nm and 660 nm wavelength pair (Table 2). Mean AAE values were calculated for all data, BB periods, and nonBB periods with the constraint that the AAE was calculated only when σ_{abs} was greater than the MDL. Lack and Langridge (2013) determined that AAE_{BC} is 1.1 ± 0.3 based on various field measurements of fossil fuel burning and urban pollution, e.g., nonBB. The mean nonBB AAE value for TAP V2010 (AAE_{TAP-V2010}: 1.31) is within this range, whereas the TAP O2010-derived value is much lower (AAE_{TAP-O2010}: 0.62). The AE33 Weingartner and Collaud Coen nonBB AAEAE33 values (1.14 and 1.13, respectively) are very close to 1.1. In contrast, the nonBB AAE_{AE33} for the Virkkula (1.74) and Drinovec (1.52) are much larger than 1.1. Histograms of the AAE values calculated for the AE33 and TAP for nonBB periods and BB periods are shown in Figs. 6 and 7, respectively.

The AAE values for V2010 corrected σ_{abs} are systematically higher than O2010 corrected σ_{abs} . The mean AAE_{TAP-V2010} for all data, BB periods, and nonBB periods are all larger than $AAE_{TAP-O2010}$ by ~0.7. A regression between $AAE_{TAP-V2010}$ and AAE_{TAP-O2010} shows a slope of 0.94 with an intercept of $0.76 (R^2 = 0.96)$. Backman et al. (2014) reported a similar observation, reporting that their derived AAE_{TAP-V2010} were higher than AAE_{TAP-O2010} by 0.57 on average for measurements on the South African Highveld, where the dominant emission source is fossil fuel burning. Backman et al. (2014) further showed that derived AAEs exhibited a pronounced dependence on the scattering wavelength of σ_{scat} (i.e., SAE). Particle size is an important driver of the scattering wavelength dependence. They found that larger SAE values increase the difference between AAE_{TAP-V2010} and AAE_{TAP-O2010}, thereby hinting at a wavelength-dependent influence of the scattering correction portion of V2010 and O2010, respectively. During our campaign the majority of the SAE values were between 2.25

and 3, and the campaign median was 2.65. This steady SAE value translates to constant scattering corrections, which then helps explain the near constant absolute difference we observe between AAE_{TAP-V2010} and AAE_{TAP-O2010}. Davies *et al.* (2019) also found V2010 AAEs to be higher than O2010 AAEs, but the difference was dependent on aerosol type. They found for V2010 AAEs to be higher than O2010 AAEs for urban emissions and aged BB by values of 0.38 and 0.33, respectively, but for fresh BB V2010 AAEs were higher than O2010 AAEs by a value of 0.77.

AAE values are commonly used to apportion absorption between BC and BrC by assuming BC has an AAE typically between 0.9 and 1.1 and that at higher wavelengths the absorption contribution by BrC becomes more dominate (Clarke *et al.*, 2007; Gyawali *et al.*, 2009; Yang *et al.*, 2009; Liu *et al.*, 2015). These assumptions are explicitly written in Eqs. (7) and (8):

$$\sigma_{absBC}(\lambda) = \sigma_{abs} (660) \times \left(\frac{\lambda}{600}\right)^{-AAE_{BC}}$$
 (7)

$$\sigma_{absBrC}(\lambda) = \sigma_{abs}(\lambda) - \sigma_{absBC}(\lambda) \tag{8}$$

Despite the large uncertainties associated with this approach (Lack and Langridge, 2013), multiple studies have found that it compares well with other methods of apportioning BC and BrC absorption (Sandradewi *et al.*, 2008; Favez *et al.*, 2010; Gianini *et al.*, 2013; Briggs and Long, 2016). One of the largest uncertainties is the choice of value to use for AAE_{BC}. As previously mentioned, Lack and Langridge (2013) determined that ambient AAE_{BC} to range from 0.8 to 1.4. In addition to the range of real AAE_{BC}, we have shown that AAE of ambient BC is operationally defined and correction specific. We used Eqs. (7) and (8) to estimate the percentage of absorption by BC ($\sigma_{absBC}/\sigma_{abs}$) and BrC ($\sigma_{absBrC}/\sigma_{abs}$) of BB periods at 470 nm for all correction schemes in Table 2. We assume only absorption by BC at 660 nm and calculate

Table 2. Mean AAE values for TAP and AE33 correction methods. Data used to calculate AAE was filtered to include only $\sigma_{abs} > MDL$.

Ŧ .	Correction scheme	AAE 470–660 nm			BrC absorption %	BrC absorption %
Instrument		All data	BB data	NonBB data	- at 470 nm assuming $AAE_{BC} = 1$	at 470 nm assuming $AAE_{BC} = AE_{nonBB}$
TAP	V2010	1.79 ± 0.70	2.47 ± 0.29	1.31 ± 0.47	60.7	67.4
TAP	O2010	1.09 ± 0.75	1.76 ± 0.30	0.62 ± 0.61	77.4	68.0
AE33	Drinovec	1.87 ± 0.56	2.35 ± 0.30	1.52 ± 0.42	63.2	75.5
AE33	Virkkula	1.97 ± 0.45	2.27 ± 0.24	1.74 ± 0.41	64.9	83.4
AE33	Weingartner	1.43 ± 0.55	1.85 ± 0.29	1.14 ± 0.49	74.8	78.3
AE33	Collaud Coen	1.43 ± 0.56	1.86 ± 0.29	1.13 ± 0.49	74.8	78.1
AE33	Arnott*	1.93 ± 0.76	2.57 ± 0.51	1.47 ± 0.55	58.6	68.9
AE33	Arnott-b**	1.88 ± 0.60	2.41 ± 0.32	1.51 ± 0.44	61.9	73.5
AE33	Schmid*	1.82 ± 0.57	2.32 ± 0.30	1.47 ± 0.44	63.9	75.0
AE33	Schmid-b**	1.83 ± 0.56	2.31 ± 0.30	1.49 ± 0.43	64.0	75.5

^{*} Arnott and Schmid: Drinovec filter-loading correction and scattering corrections using Arnott parameter values.

** Arnott-b and Schmid-b: Drinovec filter-loading correction and scattering corrections using Collaud-Coen parameter values.

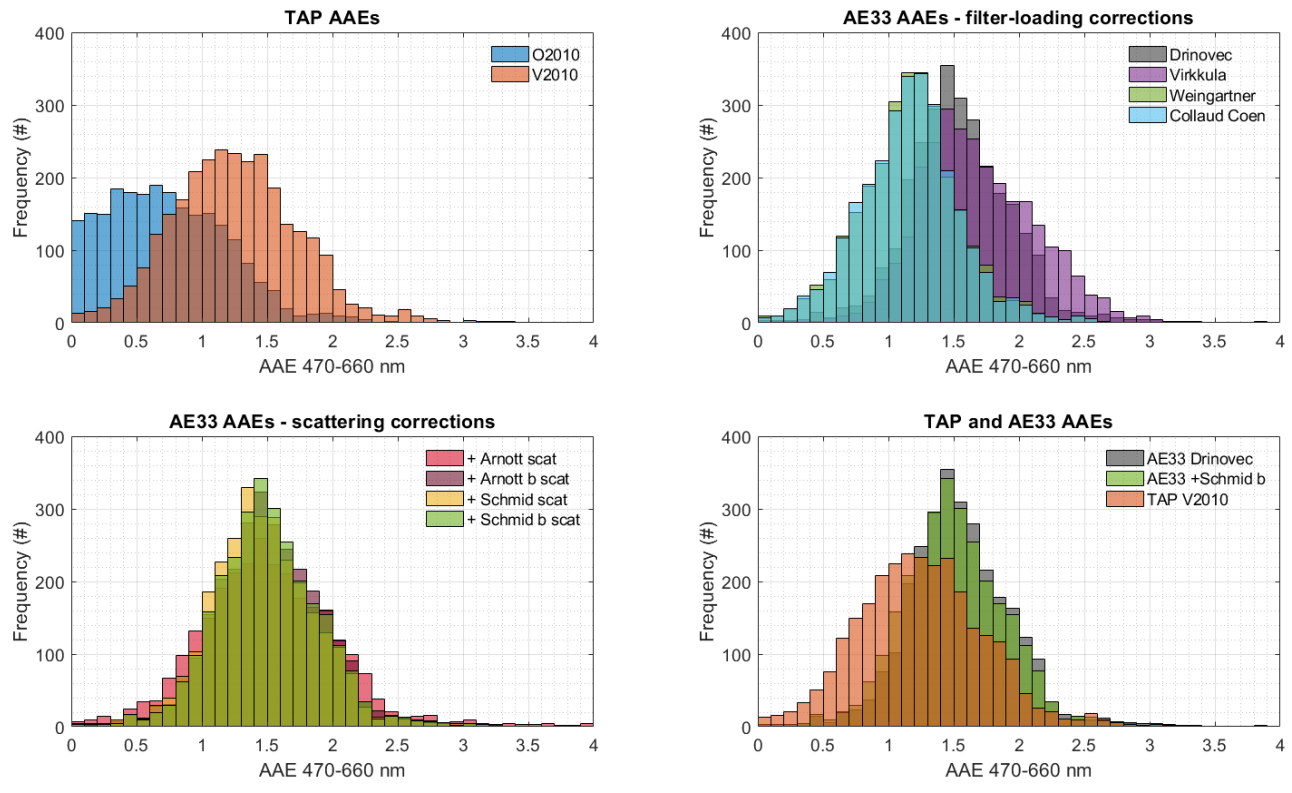


Fig. 6. Histograms of AAE calculated for nonBB periods for (1) σ_{absTAP} , (2) σ_{absAE} with different filter-loading corrections, (3) σ_{absAE} with different scattering corrections, and (4) select TAP and AE33 AAE values. Only samples that had AE33 and TAP data were used, and the data was filtered for $\sigma_{abs} > MDL$.

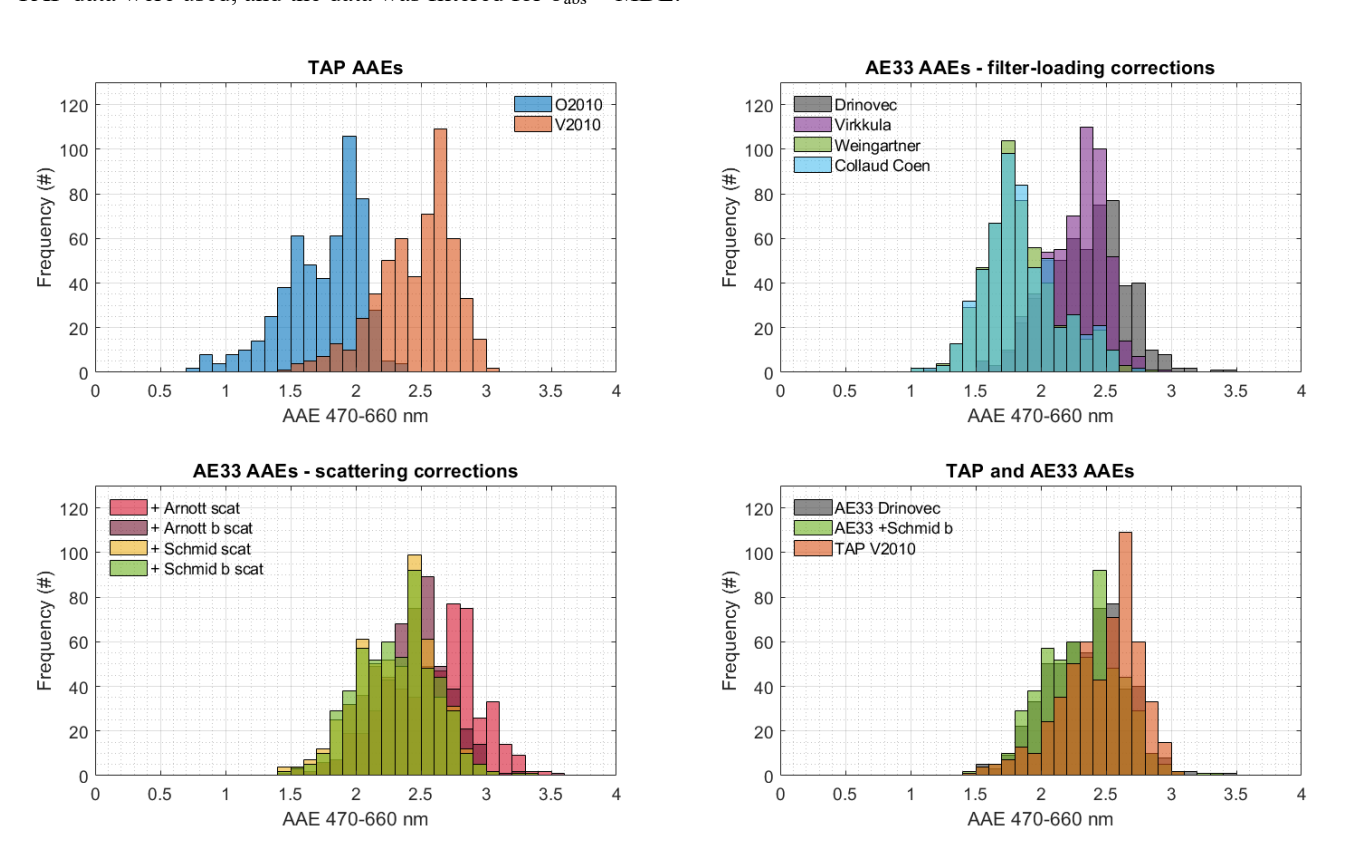


Fig. 7. Histograms of AAE calculated for BB periods for (1) σ_{absTAP} , (2) σ_{absAE} with different filter-loading corrections, (3) σ_{absAE} with different scattering corrections, and (4) select TAP and AE33 AAE values. Only samples that had AE33 and TAP data were used, and the data was filtered for $\sigma_{abs} > MDL$.

total absorption at 470 (σ_{abs}) using AAE during BB periods. We then calculated σ_{absBC} and σ_{absBrC} by (1) assuming a fixed constant AAE_{BC} and (2) setting AAE_{BC} equal to the nonBB period AAE value for that instrument and correction scheme (Table 2). Using the second method provided a good agreement between the correction methods, particularly when comparing the TAP correction methods. When assuming an AAE_{BC} = 1, the difference in BrC absorption at 470 nm for V2010 and O2010 is 17%, whereas when AAE_{BC} equals the nonBB AAE value the difference is 0.6%.

This analysis shows that AAE values for the same aerosol are different depending on the instrument and also the correction method used. This leads to a ~25% uncertainty in estimated BrC absorption values when using the AAE to determine BrC absorption.

Comparison of MACs

We calculated MACs for the TAP and AE33 as the slope of an RMA regression between σ_{abs} and rBC. The MAC

values calculated are total light absorption per unit mass BC, meaning they represent absorption by BrC and enhanced absorption by lensing in addition to BC absorption.

MAC values for TAP wavelengths for BB periods and nonBB periods are shown in Table 3. The MAC values for AE33 wavelengths for BB periods and nonBB periods are shown in Tables S3 and S4. The scatter plots of BB and nonBB σ_{absTAP-V2010} versus rBC are presented in Fig. 8. The AE33 σ_{abs} used in the MAC calculations are corrected with a C_f of 4.35. The MAC values for nonBB periods (10.1-10.7 m² g⁻¹ at 520 nm) are higher than the MAC value for fresh uncoated BC suggested by Bond and Bergstrom (2006) $(7.5 \text{ m}^2 \text{ g}^{-1} \text{ at } 550 \text{ nm}; 4.7 \text{ m}^2 \text{ g}^{-1} \text{ at } 880 \text{ nm})$. This could be due to the enhancement of absorption due to lensing effects or the additional absorption contributed by organic aerosol. Compared to measurements of ambient background air and BB-influenced air, the MAC values from this study compare well with the MAC values from previous studies. A study of 9 regional background sites in Europe using filter-based

Table 3. MAC values for TAP correction methods for BB periods and nonBB periods. The MAC values for BB periods are the slope of an RMA regression of 5-min averaged data. The MAC values for nonBB periods are the slope of an RMA regression of 1-hr averaged data.

	TAP MACs $(m^2 g^{-1})$					
Aerosol type	BB aerosol NonBB aerosol					
Correction method	V2010	O2010	V2010	O2010		
470 nm	24.1	22.7	12.9	12.3		
520 nm	15.9	16.8	10.1	10.7		
660 nm	9.24	11.19	7.68	9.00		

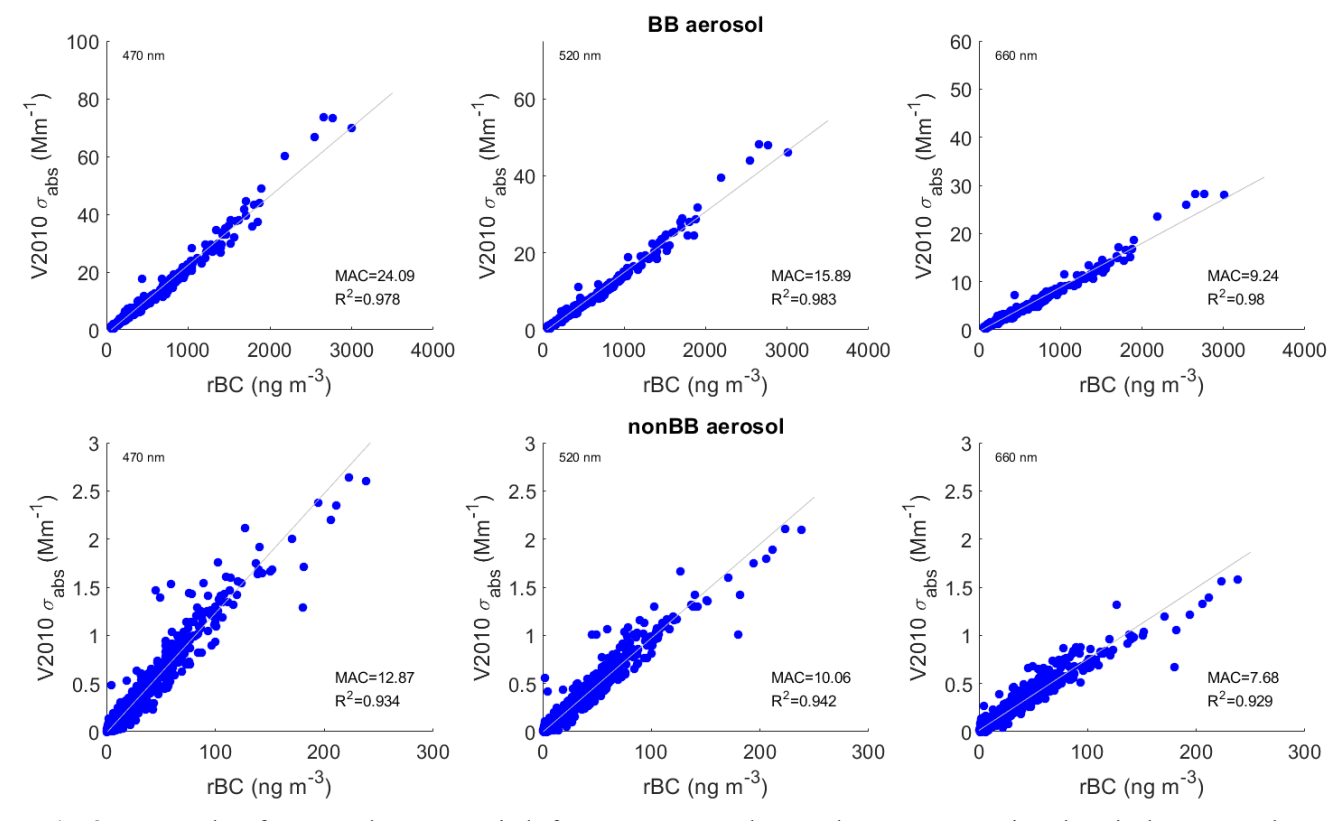


Fig. 8. Scatter plots for BB and nonBB periods for $\sigma_{absTAP-V2010}$ and rBC. The RMA regression slope is the MAC value. absorption and thermal-optical elemental carbon (EC) measurements found a MAC of 10 ± 1.33 at 637 nm to be representative of mixed boundary layer (Zanatta et al., 2016). McNaughton et al. (2011) found free troposphere air in the Arctic with some BB aerosol to have MACs of 15.4 \pm $0.4~\text{m}^2~\text{g}^{-1}$ at 470 nm, 10.9 ± 0.3 at 530 nm, and 7.4 ± 0.2 at 660 nm using a PSAP and SP2. Background continental aerosol and BB plumes measured during the 2006 Texas Air Quality Study were found to have MACs (530 nm) of 9.3 \pm 2.0 and 13.3 \pm 3.0 m² g⁻¹, respectively, using a PSAP and SP2 (Schwarz et al., 2008a).

There are a limited number of studies that have looked at MAC values of BB aerosol. Mason et al. (2018) determined unexpectedly large MAC values from BB and agricultural plumes during the SEAC4RS campaign in 2013. They determined MACs using σ_{abs} from a PAS, PSAP, and CLAP, and rBC with an SP2 at 532 nm of 21 to 26.5 m² g⁻¹, and MACs at 660 nm of 12.3 to 19.2 m² g⁻¹. These MAC values are significantly higher than the MAC values in this study and point toward the need for further investigation of MAC for BB aerosol. The high MAC values likely reflect the presence of light absorption by BrC.

Inter-comparison of BC Measurements (SP2 rBC and AE33 eBC)

While it should be noted that using a constant MAC value and conversion factor to determine eBC values from filterbased absorption measurements is inherently fraught with high uncertainty, the aethalometer is marketed as an instrument that measures BC concentrations. Because of this we compared the AE33 eBC to rBC measured by the SP2. We used the eBC concentrations output by the AE33 at 880 nm,

which uses a MAC of 7.77 m² g⁻¹ and the manufacturer's default C_{ref} value of 1.57 to convert from absorption to eBC. We compared rBC to eBC using 5-min averaged data for the BB periods and using 1-hr averaged data for nonBB periods (Fig. 9). The eBC concentrations are ~2.1 times larger than rBC for both BB and nonBB. This overestimation of eBC by aethalometers in comparison with other BC methods has been observed for various emission types. Yelverton et al. (2014) found aethalometers (AE22, AE42, and AE51) to overestimate BC from flame-generated soot by 1.75–2 times compared to MAAP, SP2, and various thermal-optical EC methods. eBC concentrations using the AE33 were consistently 1.7 times higher than thermal-optical EC for multiple urban sites in Ontario (Healy et al., 2017). Holder et al. (2016) measured field and laboratory BB emissions and found eBC (AE51) to be 2 to 2.57 times higher than rBC.

It should be noted that using the correction factor ($C_f =$ 4.35) to correct eBC results in an overcorrection with rBC now being ~20% greater than eBC. To properly align rBC and eBC, while using a MAC of 7.77 m² g⁻¹ at 880 nm, a correction factor of 3.31 is more appropriate.

CONCLUSIONS

We evaluated two filter-based absorption instruments, the AE33 and TAP, at the Mt. Bachelor Observatory (MBO, 43.98°N, 121.69°W, 2763 m a.s.l.) in central Oregon during the summer of 2016. MBO saw clean regional background air for most of the campaign apart from three days of regional BB plumes. The results and recommendations from the campaign are as follows:

The AE33's default C_{ref} value of 1.57 is too low. We

- determined a wavelength-independent correction factor (C_f) of 4.35 to use in place of a C_{ref} when calculating σ_{abs} .
- MAC values calculated using rBC derived from the SP2 and total aerosol absorption from the TAP were 24.1, 15.9, and 9.24 m² g⁻¹ for BB aerosol at 470, 520, and 660 nm, respectively, and 12.9, 10.1, and 7.68 m² g⁻¹ for nonBB aerosol at 470, 520, and 660 nm, respectively.
- AAE values exhibited a sensitivity to correction methods and were found to vary by up to 32% for BB periods and up to 65% for nonBB periods.
- AE33 eBC was ~2 times higher than rBC when using the AE33 manufacturer's settings. We recommended using a C_f of 3.31 when calculating eBC instead of the manufacturer's C_{ref} of 1.57.

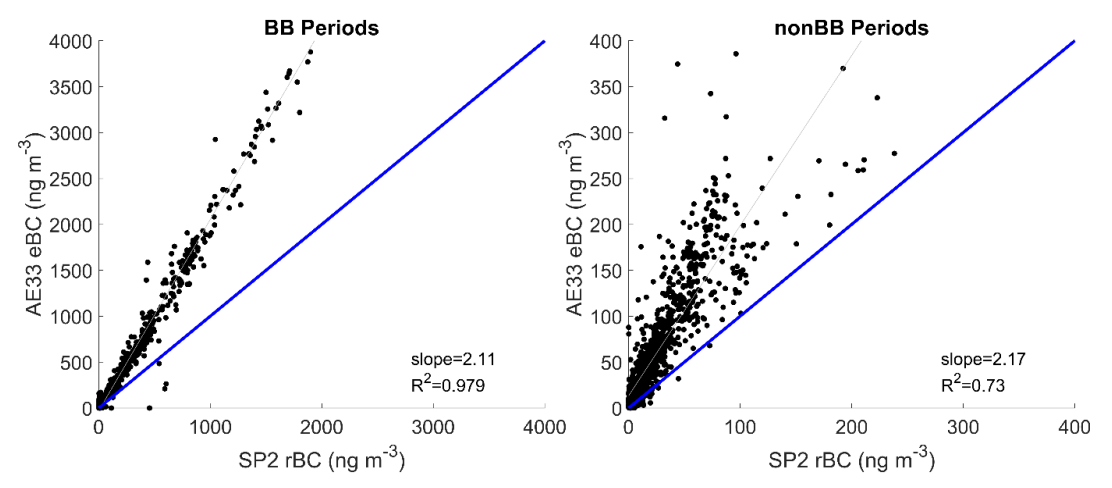


Fig. 9. SP2 rBC versus AE33 eBC for BB periods and nonBB periods. AE33 eBC values were Drinovec corrected and used the manufacturer's recommended C_{ref} of 1.57. The BB periods used 5-min averages, and the nonBB periods used 1-hr averages. The solid line is 1:1.

ACKNOWLEDGEMENTS

Research at MBO was supported by the National Science Foundation (grant number: 1447832). MBO is also supported by a grant from the NOAA Earth System Research Laboratory. The views, opinions, and findings contained in this report are those of the author(s) and should not be construed as an official National Oceanic and Atmospheric Administration or U.S. Government position, policy, or decision. We'd like to thank Betsy Andrews at NOAA for letting us to borrow the AE33 for the campaign and assisting in editing the manuscript. Researchers recognize the DOE Atmospheric Radiation Measurement (ARM) Climate Research program (contract number: 2016-6828) for use of their Single Particle Soot Photometer (SP2) for this measurement campaign. AJS gratefully acknowledges support by the U.S. DOE Office of Biological & Environmental Sciences (OBER) Atmospheric Research Program (ASR) under contracts DE-SC0012704.

SUPPLEMENTARY MATERIAL

Supplementary data associated with this article can be found in the online version at http://www.aaqr.org.

REFERENCES

Abatzoglou, J.T. and Williams, A.P. (2016). Impact of anthropogenic climate change on wildfire across western US forests. *Proc. Natl. Acad. Sci. U.S.A.* 113: 11770–11775.

Allen, G.A., Miller, P.J., Rector, L.J., Brauer, M. and Su,

J.G. (2011). Characterization of valley winter woodsmoke concentrations in Northern NY using highly time-resolved measurements. *Aerosol Air Qual. Res.* 11: 519–530.

Ambrose, J.L., Reidmiller, D.R. and Jaffe, D.A. (2011). Causes of high O₃ in the lower free troposphere over the Pacific Northwest as observed at the Mt. Bachelor Observatory. *Atmos. Environ.* 45: 5302–5315.

Anderson, T.L. and Ogren, J.A. (1998). Determining aerosol radiative properties using the TSI 3563 integrating nephelometer. *Aerosol Sci. Technol.* 29: 57–69.

Andreae, M.O. and Gelencser, A. (2006). Black carbon or brown carbon? The nature of light-absorbing carbonaceous aerosols. *Atmos. Chem. Phys.* 6: 3131–3148.

Andrews, E., Sheridan, P.J., Ogren, J.A., Hageman, D., Jefferson, A., Wendell, J., Alástuey, A., Alados-Arboledas, L., Bergin, M., Ealo, M., Hallar, A.G., Hoffer, A., Kalapov, I., Keywood, M., Kim, J., Kim, S.W., Kolonjari, F., Labuschagne, C., Lin, N.H., Macdonald, A., Mayol-Bracero, O.L., McCubbin, I.B., Pandolfi, M., Reisen, F., Sharma, S., Sherman, J.P., Sorribas, M. and Sun, J. (2019). Overview of the NOAA/ESRL federated aerosol network. *Bull. Am. Meteorol. Soc.* 100: 123–135.

Arnott, W.P., Hamasha, K., Moosmüller, H., Sheridan, P.J. and Ogren, J.A. (2005). Towards aerosol light-absorption measurements with a 7-wavelength aethalometer: Evaluation with a photoacoustic instrument and 3-wavelength nephelometer. *Aerosol Sci. Technol.* 39: 17–29.

Backman, J., Virkkula, A.O., Vakkari, V., Beukes, P., van Zyl, P., Josipovic, M., Piketh, S., Tiitta, P., Chiloane, K. and Petaja, T. (2014). Differences in aerosol absorption Ångström exponents between correction algorithms for particle soot absorption photometer measured on South

- African Highveld. Atmos. Meas. Tech. 7: 4285–4298.
- Backman, J., Schmeisser, L., Virkkula, A., Ogren, J.A., Asmi, E., Starkweather, S., Sharma, S., Eleftheriadis, K., Uttal, T. and Jefferson, A. (2017). On Aethalometer measurement uncertainties and an instrument correction factor for the Arctic. Atmos. Meas. Tech. 10: 5039–5062.
- Baylon, P., Jaffe, D.A., Wigder, N.L., Gao, H. and Hee, J. (2015). Ozone enhancement in western US wildfire plumes at the Mt. Bachelor Observatory: The role of NO_x. *Atmos. Environ.* 109: 297–304.
- Bond, T.C., Anderson, T.L. and Campbell, D. (1999). Calibration and intercomparison of filter-based measurements of visible light absorption by aerosols. *Aerosol Sci. Technol.* 30: 582–600.
- Bond, T.C. and Bergstrom, R.W. (2006). Light absorption by carbonaceous particles: An investigative review. *Aerosol Sci. Technol.* 40: 27–67.
- Bond, T.C., Habib, G. and Bergstrom, R.W. (2006). Limitations in the enhancement of visible light absorption due to mixing state. *J. Geophys. Res.* 111: D20211.
- Bond, T.C., Doherty, S.J., Fahey, D.W., Forster, P.M., Berntsen, T., DeAngelo, B.J., Flanner, M.G., Ghan, S., Kärcher, B., Koch, D., Kinne, S., Kondo, Y., Quinn, P.K., Sarofim, M.C., Schultz, M.G., Schulz, M., Venkataraman, C., Zhang, H., Zhang, S., Bellouin, N., Guttikunda, S.K., Hopke, P.K., Jacobson, M.Z., Kaiser, J.W., Klimont, Z., Lohmann, U., Schwarz, J.P., Shindell, D., Storelvmo, T., Warren, S.G. and Zender, C.S. (2013). Bounding the role of black carbon in the climate system: A scientific assessment. *J. Geophys. Res.* 118: 1–173.
- Briggs, N.L. and Long, C.M. (2016). Critical review of black carbon and elemental carbon source apportionment in Europe and the United States. *Atmos. Environ.* 144: 409–427.
- Briggs, N.L., Jaffe, D.A., Gao, H., Hee, J.R., Baylon, P.M., Zhang, Q., Zhou, S., Collier, S.C., Sampson, P.D. and Cary, R.A. (2016). Particulate matter, ozone, and nitrogen species in aged wildfire plumes observed at the Mount Bachelor Observatory. *Aerosol Air Qual. Res.* 16: 3075–3087.
- Brock, C.A., Cozic, J., Bahreini, R., Froyd, K.D., Middlebrook, A.M., McComiskey, A., Brioude, J., Cooper, O., Stohl, A. and Aikin, K. (2011). Characteristics, sources, and transport of aerosols measured in spring 2008 during the aerosol, radiation, and cloud processes affecting Arctic Climate (ARCPAC) Project. *Atmos. Chem. Phys.* 11: 2423–2453.
- Cappa, C.D., Lack, D.A., Burkholder, J.B. and Ravishankara, A. (2008). Bias in filter-based aerosol light absorption measurements due to organic aerosol loading: Evidence from laboratory measurements. *Aerosol Sci. Technol.* 42: 1022–1032.
- Cappa, C.D., Kolesar, K.R., Zhang, X., Atkinson, D.B., Pekour, M.S., Zaveri, R.A., Zelenyuk, A. and Zhang, Q. (2016). Understanding the optical properties of ambient sub- and supermicron particulate matter: Results from the CARES 2010 field study in northern California. *Atmos. Chem. Phys.* 16: 6511–6535.
- Clarke, A., McNaughton, C., Kapustin, V., Shinozuka, Y.,

- Howell, S., Dibb, J., Zhou, J., Anderson, B., Brekhovskikh, V. and Turner, H. (2007). Biomass burning and pollution aerosol over North America: Organic components and their influence on spectral optical properties and humidification response. *J. Geophys. Res.* 112: D12S18,.
- Collaud Coen, M., Weingartner, E., Apituley, A., Ceburnis,
 D., Fierz-Schmidhauser, R., Flentje, H., Henzing, J.,
 Jennings, S.G., Moerman, M. and Petzold, A. (2010).
 Minimizing light absorption measurement artifacts of the
 Aethalometer: Evaluation of five correction algorithms.
 Atmos. Meas. Tech. 3: 457–474.
- Collier, S., Zhou, S., Onasch, T.B., Jaffe, D.A., Kleinman, L., Sedlacek III, A.J., Briggs, N.L., Hee, J., Fortner, E. and Shilling, J.E. (2016). Regional influence of aerosol emissions from wildfires driven by combustion efficiency: Insights from the BBOP campaign. *Environ. Sci. Technol.* 50: 8613–8622.
- Davies, N.W., Fox, C., Szpek, K., Cotterell, M.I., Taylor, J.W., Allan, J.D., Williams, P.I., Trembath, J., Haywood, J.M. and Langridge, J.M. (2019). Evaluating biases in filter-based aerosol absorption measurements using photoacoustic spectroscopy. *Atmos. Meas. Tech.* 12: 3417–3434.
- Dennison, P.E., Brewer, S.C., Arnold, J.D. and Moritz, M.A. (2014). Large wildfire trends in the western United States, 1984–2011. *Geophys. Res. Lett.* 41: 2928–2933.
- Drinovec, L., Močnik, G., Zotter, P., Prévôt, A., Ruckstuhl, C., Coz, E., Rupakheti, M., Sciare, J., Müller, T. and Wiedensohler, A. (2015). The "dual-spot" Aethalometer: An improved measurement of aerosol black carbon with real-time loading compensation. *Atmos. Meas. Tech.* 8: 1965–1979.
- Favez, O., Haddad, I.E., Piot, C., Boréave, A., Abidi, E., Marchand, N., Jaffrezo, J.L., Besombes, J.L., Personnaz, M.-B. and Sciare, J. (2010). Inter-comparison of source apportionment models for the estimation of wood burning aerosols during wintertime in an Alpine city (Grenoble, France). Atmos. Chem. Phys. 10: 5295–5314.
- Fischer, E.V., Jaffe, D.A., Marley, N.A., Gaffney, J.S. and Marchany-Rivera, A. (2010a). Optical properties of aged Asian aerosols observed over the US Pacific Northwest. *J. Geophys. Res.* 115: D20209.
- Fischer, E.V., Jaffe, D.A., Reidmiller, D.R. and Jaeglé, L. (2010b). Meteorological controls on observed peroxyacetyl nitrate at Mount Bachelor during the spring of 2008. *J. Geophys. Res.* 115: D03302.
- Gianini, M., Piot, C., Herich, H., Besombes, J.L., Jaffrezo, J.L. and Hueglin, C. (2013). Source apportionment of PM₁₀, organic carbon and elemental carbon at Swiss sites: An intercomparison of different approaches. *Sci. Total Environ.* 454: 99–108.
- Gratz, L.E., Jaffe, D.A. and Hee, J.R. (2015). Causes of increasing ozone and decreasing carbon monoxide in springtime at the Mt. Bachelor Observatory from 2004 to 2013. *Atmos. Environ.* 109: 323–330.
- Gyawali, M., Arnott, W., Lewis, K. and Moosmüller, H. (2009). In situ aerosol optics in Reno, NV, USA during and after the summer 2008 California wildfires and the influence of absorbing and non-absorbing organic coatings

- on spectral light absorption. *Atmos. Chem. Phys.* 9: 8007–8015.
- Hansen, A., Rosen, H. and Novakov, T. (1984). The aethalometer—an instrument for the real-time measurement of optical absorption by aerosol particles. *Sci. Total Environ.* 36: 191–196.
- Healy, R.M., Sofowote, U., Su, Y., Debosz, J., Noble, M., Jeong, C.H., Wang, J., Hilker, N., Evans, G. and Doerksen, G. (2017). Ambient measurements and source apportionment of fossil fuel and biomass burning black carbon in Ontario. *Atmos. Environ.* 161: 34–47.
- Holder, A.L., Hagler, G.S., Aurell, J., Hays, M.D. and Gullett, B.K. (2016). Particulate matter and black carbon optical properties and emission factors from prescribed fires in the southeastern United States. *J. Geophys. Res.* 121: 3465–3483.
- Jaffe, D., Prestbo, E., Swartzendruber, P., Weiss-Penzias, P., Kato, S., Takami, A., Hatakeyama, S. and Kajii, Y. (2005). Export of atmospheric mercury from Asia. *Atmos. Environ*. 39: 3029–3038.
- Kim, J.H., Kim, S.W., Ogren, J.A., Sheridan, P.J., Yoon, S.C., Sharma, S. and Lin, N.H. (2018). Multiple scattering correction factor estimation for aethalometer aerosol absorption coefficient measurement. *Aerosol Sci. Technol*. 53: 160–171.
- Kirchstetter, T.W., Novakov, T. and Hobbs, P.V. (2004). Evidence that the spectral dependence of light absorption by aerosols is affected by organic carbon. *J. Geophys. Res.* 109: D21208.
- Kondo, Y., Sahu, L., Kuwata, M., Miyazaki, Y., Takegawa, N., Moteki, N., Imaru, J., Han, S., Nakayama, T. and Oanh, N.K. (2009). Stabilization of the mass absorption cross section of black carbon for filter-based absorption photometry by the use of a heated inlet. *Aerosol Sci. Technol.* 43: 741–756.
- Laborde, M., Crippa, M., Tritscher, T., Jurányi, Z., Decarlo, P., Temime-Roussel, B., Marchand, N., Eckhardt, S., Stohl, A. and Baltensperger, U. (2013). Black carbon physical properties and mixing state in the European megacity Paris. Atmos. Chem. Phys. 13: 5831–5856.
- Lack, D.A., Cappa, C.D., Covert, D.S., Baynard, T., Massoli, P., Sierau, B., Bates, T.S., Quinn, P.K., Lovejoy, E.R. and Ravishankara, A. (2008). Bias in filter-based aerosol light absorption measurements due to organic aerosol loading: Evidence from ambient measurements. *Aerosol Sci. Technol.* 42: 1033–1041.
- Lack, D.A., Langridge, J., Bahreni, R., Cappa, C.D., Middlebrook, A. and Schwarz, J.P. (2012). Brown carbon and internal mixing in biomass burning particles. *Proc. Natl. Acad. Sci. U.S.A.* 10: 14802–14807.
- Lack, D.A. and Langridge, J.M. (2013). On the attribution of black and brown carbon light absorption using the Ångström exponent. *Atmos. Chem. Phys.* 13: 10535–10543.
- Laing, J.R., Jaffe, D.A. and Hee, J.R. (2016). Physical and optical properties of aged biomass burning aerosol from wildfires in Siberia and the Western USA at the Mt. Bachelor Observatory. *Atmos. Chem. Phys.* 16: 15185–15197
- Liu, J., Scheuer, E., Dibb, J., Diskin, G., Ziemba, L.,

- Thornhill, K., Anderson, B., Wisthaler, A., Mikoviny, T. and Devi, J. (2015). Brown carbon aerosol in the North American continental troposphere: Sources, abundance, and radiative forcing. *Atmos. Chem. Phys.* 15: 7841–7858.
- Mason, B., Wagner, N., Adler, G., Andrews, E., Brock, C., Gordon, T., Lack, D., Perring, A., Richardson, M. and Schwarz, J. (2018). An intercomparison of aerosol absorption measurements conducted during the SEAC4RS campaign. *Aerosol Sci. Technol.* 52: 1012–1027.
- McNaughton, C., Clarke, A., Freitag, S., Kapustin, V., Kondo, Y., Moteki, N., Sahu, L., Takegawa, N., Schwarz, J. and Spackman, J. (2011). Absorbing aerosol in the troposphere of the Western Arctic during the 2008 ARCTAS/ARCPAC airborne field campaigns. *Atmos. Chem. Phys.* 11: 7561–7582.
- Moosmuller, H., Chakrabarty, R.K. and Arnott, W.P. (2009). Aerosol light absorption and its measurement: A review. *J. Quant. Spectrosc. Radiat. Transfer* 110: 844–878.
- Moteki, N. and Kondo, Y. (2007). Effects of mixing state on black carbon measurements by laser-induced incandescence. *Aerosol Sci. Technol.* 41: 398–417.
- Moteki, N. and Kondo, Y. (2010). Dependence of laser-induced incandescence on physical properties of black carbon aerosols: Measurements and theoretical interpretation. *Aerosol Sci. Technol.* 44: 663–675.
- Moteki, N., Kondo, Y., Nakayama, T., Kita, K., Sahu, L.K., Ishigai, T., Kinase, T. and Matsumi, Y. (2010). Radiative transfer modeling of filter-based measurements of light absorption by particles: Importance of particle size dependent penetration depth. *J. Aerosol Sci.* 41: 401–412.
- Müller, T., Virkkula, A. and Ogren, J. (2014). Constrained two-stream algorithm for calculating aerosol light absorption coefficient from the Particle Soot Absorption Photometer. *Atmos. Meas. Tech.* 7: 4049–4070.
- Müller, T. (2015). Development of correction factors for Aethalometers AE31 and AE33. In Proceedings of the ACTRIS-2 WP3 Workshop, 2015, Athens, Greece, pp. 10–12.
- Myhre, G., Shindell, D., Bréon, F.M., Collins, W., Fuglestvedt, J., Huang, J., Koch, D., Lamarque, J.F., Lee, D., Mendoza, B., Nakajima, T., Robock, A., G. Stephens, Takemura, T. and Zhang, H. (2013). Anthropogenic and Natural Radiative Forcing. In *Climate Change 2013: The Physical Science Basis. Contribution of Working Group I to the Fifth Assessment Report of the Intergovernmental Panel on Climate Change*, Stocker, T.F., Qin, D., Plattner, G.K., Tignor, M., Allen, S.K., Boschung, J., Nauels, A., Xia, Y., Bex, V. and Midgley, P.M. (Eds.), Cambridge University Press, Cambridge, United Kingdom.
- Nakayama, T., Kondo, Y., Moteki, N., Sahu, L., Kinase, T., Kita, K. and Matsumi, Y. (2010). Size-dependent correction factors for absorption measurements using filter-based photometers: PSAP and COSMOS. *J. Aerosol Sci.* 41: 333–343.
- Ogren, J.A. (2010). Comment on "Calibration and intercomparison of filter-based measurements of visible light absorption by aerosols". *Aerosol Sci. Technol.* 44: 589–591.
- Ogren, J.A., Wendell, J., Andrews, E. and Sheridan, P.J.

- (2017). Continuous light absorption photometer for long-term studies. *Atmos. Meas. Tech.* 10: 4805–4818.
- Petzold, A., Ogren, J.A., Fiebig, M., Laj, P., Li, S.M., Baltensperger, U., Holzer-Popp, T., Kinne, S., Pappalardo, G., Sugimoto, N., Wehrli, C., Wiedensohler, A. and Zhang, X.Y. (2013). Recommendations for reporting "black carbon" measurements. *Atmos. Chem. Phys.* 13: 8365–8379.
- Rajesh, T. and Ramachandran, S. (2018). Black carbon aerosol mass concentration, absorption and single scattering albedo from single and dual spot aethalometers: Radiative implications. *J. Aerosol Sci.* 119: 77–90.
- Ran, L., Deng, Z., Wang, P. and Xia, X. (2016). Black carbon and wavelength-dependent aerosol absorption in the North China Plain based on two-year aethalometer measurements. *Atmos. Environ.* 142: 132–144.
- Reidmiller, D.R., Jaffe, D.A., Fischer, E.V. and Finley, B. (2010). Nitrogen oxides in the boundary layer and free troposphere at the Mt. Bachelor Observatory. *Atmos. Chem. Phys.* 10: 6043–6062.
- Saleh, R., Hennigan, C.J., McMeeking, G.R., Chuang, W.K., Robinson, E.S., Coe, H., Donahue, N.M. and Robinson, A.L. (2013). Absorptivity of brown carbon in fresh and photo-chemically aged biomass-burning emissions. *Atmos. Chem. Phys.* 13: 7683–7693.
- Sandradewi, J., Prévôt, A.S., Szidat, S., Perron, N., Alfarra, M.R., Lanz, V.A., Weingartner, E. and Baltensperger, U. (2008). Using aerosol light absorption measurements for the quantitative determination of wood burning and traffic emission contributions to particulate matter. *Environ. Sci. Technol.* 42: 3316–3323.
- Saturno, J., Pöhlker, C., Massabò, D., Brito, J., Carbone, S., Cheng, Y., Chi, X., Ditas, F., de Angelis, I.H. and Morán-Zuloaga, D. (2017). Comparison of different Aethalometer correction schemes and a reference multi-wavelength absorption technique for ambient aerosol data. *Atmos. Meas. Tech.* 10: 2837.
- Schmid, O., Artaxo, P., Arnott, W., Chand, D., Gatti, L.V., Frank, G., Hoffer, A., Schnaiter, M. and Andreae, M. (2006). Spectral light absorption by ambient aerosols influenced by biomass burning in the Amazon Basin. I: Comparison and field calibration of absorption measurement techniques. *Atmos. Chem. Phys.* 6: 3443–3462.
- Schwarz, J., Gao, R.S., Fahey, D.W., Thomson, D.S., Watts, L.A., Wilson, J.C., Reeves, J.M., Darbeheshti, M., Baumgardner, D.G., Kok, G.L., Chung, S.H., Schulz, M., Hendricks, J., Lauer, A., Karcher, B., Slowik, J.G., Rosenlof, K.H., Thompson, T.L., Langford, A.O., Loewenstein, M. and Aikin, K.C. (2006). Single-particle measurements of midlatitude black carbon and light-scattering aerosols from the boundary layer to the lower stratosphere. J. Geophys. Res. 111: D16207.
- Schwarz, J., Gao, R., Spackman, J., Watts, L., Thomson, D., Fahey, D., Ryerson, T., Peischl, J., Holloway, J. and Trainer, M. (2008a). Measurement of the mixing state, mass, and optical size of individual black carbon particles in urban and biomass burning emissions. *Geophys. Res. Lett.* 35: L13810.
- Schwarz, J., Spackman, J., Fahey, D., Gao, R., Lohmann, U., Stier, P., Watts, L., Thomson, D., Lack, D. and Pfister,

- L. (2008b). Coatings and their enhancement of black carbon light absorption in the tropical atmosphere. *J. Geophys. Res.* 113: D03203.
- Segura, S., Estellés, V., Titos, G., Lyamani, H., Utrillas, M., Zotter, P., Prévôt, A., Mocnik, G., Alados-Arboledas, L. and Martínez-Lozano, J. (2014). Determination and analysis of in situ spectral aerosol optical properties by a multi-instrumental approach. *Atmos. Meas. Tech.* 7: 2373.
- Segura, S., Estellés, V., Esteve, A., Marcos, C., Utrillas, M. and Martínez-Lozano, J. (2016). Multiyear in-situ measurements of atmospheric aerosol absorption properties at an urban coastal site in western Mediterranean. *Atmos. Environ.* 129: 18–26.
- Springston, S.R. and Sedlacek III, A.J. (2007). Noise characteristics of an instrumental particle absorbance technique. *Aerosol Sci. Technol.* 41: 1110–1116.
- Stephens, M., Turner, N. and Sandberg, J. (2003). Particle identification by laser-induced incandescence in a solid-state laser cavity. *Appl. Opt.* 42: 3726–3736.
- Subramanian, R., Roden, C.A., Boparai, P. and Bond, T.C. (2007). Yellow beads and missing particles: Trouble ahead for filter-based absorption measurements. *Aerosol Sci. Technol.* 41: 630–637.
- Taylor, J., Allan, J., Allen, G., Coe, H., Williams, P., Flynn, M., Le Breton, M., Muller, J., Percival, C. and Oram, D. (2014). Size-dependent wet removal of black carbon in Canadian biomass burning plumes. *Atmos. Chem. Phys.* 14: 13755–13771.
- Timonen, H., Wigder, N. and Jaffe, D. (2013). Influence of background particulate matter (PM) on urban air quality in the Pacific Northwest. *J Environ. Manage.* 129: 333–340.
- Timonen, H., Jaffe, D.A., Wigder, N., Hee, J., Gao, H., Pitzman, L. and Cary, R.A. (2014). Sources of carbonaceous aerosol in the free troposphere. *Atmos. Environ.* 92: 146–153.
- Virkkula, A., Ahlquist, N.C., Covert, D.S., Arnott, W.P., Sheridan, P.J., Quinn, P.K. and Coffman, D.J. (2005). Modification, calibration and a field test of an instrument for measuring light absorption by particles. *Aerosol Sci. Technol.* 39: 68–83.
- Virkkula, A., Mäkelä, T., Hillamo, R., Yli-Tuomi, T., Hirsikko, A., Hämeri, K. and Koponen, I.K. (2007). A simple procedure for correcting loading effects of aethalometer data. J. Air Waste Manage. Assoc. 57: 1214–1222.
- Virkkula, A. (2010). Correction of the Calibration of the 3-wavelength Particle Soot Absorption Photometer (3 PSAP). Aerosol Sci. Technol. 44: 706–712.
- Wang, J., Virkkula, A., Gao, Y., Lee, S., Shen, Y., Chi, X., Nie, W., Liu, Q., Xu, Z., Huang, X., Wang, T., Cui, L. and Ding, A. (2017). Observations of aerosol optical properties at a coastal site in Hong Kong, South China. *Atmos. Chem. Phys.* 17: 2653–2671.
- Weingartner, E., Saathoff, H., Schnaiter, M., Streit, N., Bitnar, B. and Baltensperger, U. (2003). Absorption of light by soot particles: Determination of the absorption coefficient by means of aethalometers. *J. Aerosol Sci.* 34: 1445–1463.
- Weiss-Penzias, P., Jaffe, D.A., Swartzendruber, P., Dennison,

- J.B., Chand, D., Hafner, W. and Prestbo, E. (2006). Observations of Asian air pollution in the free troposphere at Mount Bachelor Observatory during the spring of 2004. *J. Geophys. Res.* 111: D10304.
- Weiss-Penzias, P., Jaffe, D., Swartzendruber, P., Hafner, W., Chand, D. and Prestbo, E. (2007). Quantifying Asian and biomass burning sources of mercury using the Hg/CO ratio in pollution plumes observed at the Mount Bachelor Observatory. *Atmos. Environ.* 41: 4366–4379.
- Wigder, N.L., Jaffe, D.A. and Saketa, F.A. (2013). Ozone and particulate matter enhancements from regional wildfires observed at Mount Bachelor during 2004–2011. *Atmos. Environ.* 75: 24–31.
- Yang, M., Howell, S., Zhuang, J. and Huebert, B. (2009). Attribution of aerosol light absorption to black carbon, brown carbon, and dust in China interpretations of atmospheric measurements during EAST-AIRE. *Atmos. Chem. Phys.* 9: 2035–2050.
- Yelverton, T.L., Hays, M.D., Gullett, B.K. and Linak, W.P. (2014). Black carbon measurements of flame-generated soot as determined by optical, thermal-optical, direct absorption, and laser incandescence methods. *Environ*.

- Eng. Sci. 31: 209-215.
- Zanatta, M., Gysel, M., Bukowiecki, N., Müller, T., Weingartner, E., Areskoug, H., Fiebig, M., Yttri, K.E., Mihalopoulos, N. and Kouvarakis, G. (2016). A European aerosol phenomenology-5: Climatology of black carbon optical properties at 9 regional background sites across Europe. *Atmos. Environ.* 145: 346–364.
- Zhang, L. and Jaffe, D.A. (2017). Trends and sources of ozone and sub-micron aerosols at the Mt. Bachelor Observatory (MBO) during 2004–2015. *Atmos. Environ*. 165: 143–154.
- Zhou, S., Collier, S., Jaffe, D.A., Briggs, N.L., Hee, J., Sedlacek III, A.J., Kleinman, L., Onasch, T.B. and Zhang, Q. (2017). Regional influence of wildfires on aerosol chemistry in the western US and insights into atmospheric aging of biomass burning organic aerosol. *Atmos. Chem. Phys.* 17: 2477–2493.

Received for review, June 11, 2019 Revised, September 25, 2019 Accepted, October 2, 2019

Comparison of Filter-Based Absorption Measurements of Biomass Burning Aerosol and Background Aerosol at the Mt. Bachelor **Observatory**

James R. Laing¹, Daniel A. Jaffe^{1,2*}, Arthur J. Sedlacek, III³
¹University of Washington Bothell, Bothell, Washington, USA.

Supplement

* Corresponding author: Daniel A. Jaffe, djaffe@uw.edu

²University of Washington, Seattle, Washington, USA.

³Brookhaven National Laboratory, Upton, New York, USA.

Table Titles

- Table S2. Aerosol instrumentation and correction schemes.
- Table S2. SSA values measured at 520 nm for TAP and AE33 correction methods using all data. Data was filtered if $\sigma_{abs} < 2*MDL$ or $\sigma_{scat} < 1$ Mm⁻¹.
- Table S3. MAC values for AE33 correction methods for BB periods. A C_f = 4.35 was used for all σ_{absAE} . The MAC values are the slope of an RMA regression of 5-min averaged data.
- Table S4. MAC values for AE33 correction methods for nonBB periods. A C_f = 4.35 was used for all σ_{absAE} . The MAC values are the slope of an RMA regression of 1-hr averaged data.

Table S1.

Instrument	Correction type	Correction name	Correction scheme	Reference
TAP	Filter loading, Scattering effects of loaded aerosol	V2010	$\sigma_{abs,n} = f(Tr) * \sigma_{ATN,n} - s_v * \sigma_{scat,n}$ Where $f(Tr) \text{ is the filter-loading correction and } s_v * \sigma_{(scat,n)} \text{ is the scattering correction}$ $f(Tr) = (k_0 + k_1 * h(SSA)) * ln(Tr)$ Tr is the filter transmittance, $k_0, k_1, s_v, h_0, h_1 \text{ wavelength-dependent values were}$	Virkkula <i>et al.</i> (2005) Virkkula (2010)
TAP	Filter loading, Scattering effects of loaded aerosol	O2010	taken from Table 1 in Virkkula (2010). $\sigma_{abs,n} = f(Tr)\sigma_{ATN,n} - s_o * \sigma_{scat,n}$ Where $f(Tr) \text{ is the filter-loading correction and } s_o * \sigma_{(scat,n)} \text{ is the scattering correction} f(Tr) = \frac{0.85}{K_2(1.0796*Tr+0.71)}$ $s_o = \frac{K_1}{K_2}, \text{ K}_1 = 0.02 \text{ and K}_2 = 1.22$	Bond et al. (1999) Ogren (2010)
AE33	Filter loading	Drinovec (R _D)	$\sigma_{abs,n} = \frac{\sigma_{ATN,n}}{C_{ref} * R_{D,n}}$ Where $R_{D,n} = (1 - k_D * ATN)$ And k _D is the compensation factor derived from the real-time dual-spot algorithm in the AE33.	Drinovec et al. (2015)
AE33	Filter loading	Virkkula (Rv)	$\sigma_{abs,n} = \frac{\sigma_{ATN,n}}{C_{ref} * R_{V,n}}$ Where $R_{V,n} = \frac{1}{(1 + k_i * ATN)}$ ki is calculated by aligning the last measurement on filter spot t-1 with the first measurement on filter spot t.	Virkkula et al. (2007)
AE33	Filter loading	Weingartner (Rw)	$\sigma_{abs,n} = \frac{\sigma_{ATN,n}}{C_{ref} * R_{w,n}}$ Where	Weingartner et al. (2003)

			$R_{w,n} = \left(\frac{1}{f} - 1\right) * \frac{\ln ATN_n - \ln(10\%)}{\ln(50\%) - \ln(10\%)} + 1$ $f = m * (1 - SSA) + 1$ and m = (0.87 to 0.85)	
AE33	Filter loading	Collaud Coen (Rc)	$\sigma_{abs,n} = \frac{\sigma_{ATN,n}}{C_{ref} * R_{C,n}}$ Where $R_{C,n} = \left(\frac{1}{m*(1-SSA_{0,s,n})+1}-1\right)*\frac{ATN_n}{50\%}+1$ ATN _n is filter attenuation as a percentage, SSA _{0,s,n} is mean SSA since the last filter spot change.	Collaud Coen et al. (2010)
AE33	Scattering effects of loaded aerosol	Arnott	$\sigma_{abs,n} = \frac{\sigma_{atn,n} - \alpha(\lambda) * \sigma_{scat,n}}{C_{ref} * R_n}$ Where R is a filter-loading correction factor, $\alpha(\lambda) \text{ is parameter for scattering correction from Arnott}$ $et al. (2005).$	Arnott et al. (2005)
AE33	Scattering effects of loaded aerosol	Arnott-b	$\sigma_{abs,n} = \frac{\sigma_{atn,n} - \alpha_{new} * \sigma_{scat,s,n}}{C_{ref} * R_n}$ Where R is a filter-loading correction factor, $\sigma_{scat,s,n}$ is the mean σ_{scat} since the last filter spot change, α_{new} is parameter for scattering correction from Collaud Coen <i>et al.</i> (2010).	Collaud Coen et al. (2010)
AE33	Scattering effects of loaded aerosol	Schmid	$\sigma_{abs,n} = \frac{\sigma_{ATN,n}}{(C_{ref} + C_{scat,n}) * R_n}$ Where $C_{scat,n} = \alpha(\lambda) * \frac{SSA}{1 - SSA}$ $\alpha(\lambda) \text{ is parameter for scattering correction from Arnott}$ $et al. (2005),$	(Schmid et al., 2006)

			SSA _{0,s,n} is mean SSA since the last filter spot change.	
AE33	Scattering effects of loaded aerosol	Schmid-b	$\sigma_{abs,n} = \frac{\sigma_{ATN,n}}{(C_{ref} + C_{scat,n,new}) * R_n}$ Where $C_{scat,n,new} = \alpha_{new} * \frac{SSA_{0,s,n}}{1 - SSA_{0,s,n}}$ $\alpha_{new} \text{ is parameter for scattering correction from Collaud}$	Collaud Coen et al. (2010)
			Coen et al. (2010),	
			SSA _{0,s,n} is mean SSA since the last filter spot change.	

Table S2

Instrument	Correction scheme	Mean SSA	Median SSA	stdev
TAP	V2010	0.943	0.946	0.024
TAP	O2010	0.946	0.949	0.024
AE33	Drinovec (R _D)	0.937	0.942	0.023
AE33	Virkkula (R _V)	0.939	0.943	0.026
AE33	Weingartner (R _W)	0.944	0.949	0.022
AE33	Collaud Coen (R _C)	0.944	0.949	0.022
AE33	Arnott	0.950	0.955	0.023
AE33	Arnott-b	0.941	0.946	0.024
AE33	Schmid	0.948	0.952	0.023
AE33	Schmid-b	0.941	0.946	0.023

Table S3

		MAC BB (m ² g ⁻¹)						
Instrument	Correction scheme	370 nm	470 nm	520 nm	660 nm	880 nm	950 nm	
AE33	σ_{abs} Drinovec	59.2	25.8	18.0	10.6	6.16	5.68	
AE33	σ _{abs} Virkkula	57.1	25.9	18.4	10.9	6.45	6.00	
AE33	σ_{abs} Weingartner	45.6	20.3	15.2	9.73	6.20	5.81	
AE33	σ _{abs} Collaud Coen	47.4	21.0	15.7	10.0	6.35	5.94	
AE33	σ _{abs} Arnott*	51.7	20.5	13.7	7.39	3.88	3.57	
AE33	σ_{abs} Arnott-b**	57.1	24.9	17.4	10.2	5.95	5.50	
AE33	σ _{abs} Schmid*	46.8	20.7	14.4	8.44	4.90	4.51	
AE33	σ _{abs} Schmid-b**	54.4	24.1	16.9	10.0	5.87	5.42	

^{*} Arnott and Schmid: Drinovec filter-loading correction and scattering correction using Arnott parameter values.

** Arnott-b and Schmid-b: Drinovec filter-loading correction and scattering correction using Collaud-Coen

parameter values.

Table S4

		MAC nonBB (m ² g ⁻¹)					
Instrument	Correction scheme	370 nm	470 nm	520 nm	660 nm	880 nm	950 nm
AE33	σ _{abs} Drinovec	25.8	14.8	12.1	8.74	6.09	5.79
AE33	σ _{abs} Virkkula	26.1	15.8	12.6	8.54	5.81	5.80
AE33	σ_{abs} Weingartner	22.7	12.5	10.5	8.17	6.38	6.19
AE33	σ _{abs} Collaud Coen	22.9	12.8	10.8	8.45	6.55	6.35
AE33	σ _{abs} Arnott*	21.4	11.6	9.35	6.89	4.94	4.76
AE33	σ_{abs} Arnott-b**	24.7	14.4	11.7	8.48	5.92	5.64
AE33	σ _{abs} Schmid*	20.7	11.6	9.42	6.83	4.82	4.60
AE33	σ _{abs} Schmid-b**	23.0	13.4	10.9	7.99	5.63	5.37

^{*} Arnott and Schmid: Drinovec filter-loading correction and scattering correction using Arnott parameter values.

** Arnott-b and Schmid-b: Drinovec filter-loading correction and scattering correction using Collaud-Coen

parameter values.

Figure captions

- **Fig. S1.** Comparison of V2010 and O2010 σ_{absTAP} with and without the scattering correction using 5-min averages. The solid line is 1:1.
- Fig. S2. Comparison of σ_{absAE} filter-loading correction for (1) Virkkula versus Drinovec corrections, (2) Weingartner versus Drinovec corrections, and (3) Collaud Coen versus Drinovec corrections for all 7 wavelengths using 5-min averages. The solid line is 1:1.
- Fig. S3. Comparison of σ_{absAE} with and without scattering corrections for the Arnott scattering correction method using (1) Arnott parameters and (2) Collaud Coen parameters using 5-min averages. The solid line is 1:1.
- **Fig. S4**. Comparison of σ_{absAE} with and without scattering corrections for the Schmid scattering correction method using (1) Arnott parameters and (2) Collaud Coen parameters using all 5-min averages. The solid line is 1:1.
- **Fig. S5.** Aethalometer correction factors (C_f) for 470, 520, and 660 nm as a function of TAP AAE calculated for the 470–660 nm wavelength pair. The TAP AAE values were calculated using the V2010 corrected σ_{absTAP} . The grey dots are all of the data points, the black squares represent the median values, the red circles are the 25th and 75th percentile values, and the blue diamonds are the 5th and 95th percentile values.
- **Fig. S6.** Aethalometer correction factors (C_f) for 470, 520 ,and 660 nm as a function of SSA. The SSA values were calculated using V2010 corrected σ_{absTAP} at 520 nm. The symbols characterization is the same as in Fig. S5.
- **Fig. S7.** Aethalometer correction factors (C_f) for 470, 520, and 660 nm as a function of aethalometer ATN values. The plot is colored by sample density.
- **Fig. S8.** Scatter plot of SSA (520 nm) versus AAE (470–660 nm) for all 5-min data points colored by aethalometer correction factors (C_f) for 470, 520, and 660 nm. The SSA and AAE values were calculated using V2010 corrected σ_{absTAP} .
- Fig. S9. Comparison of σ_{absAE} with (1) Drinovec and (2) Virkkula filter-loading corrections with σ_{absTAP} using all 5-min averages. A $C_f = 4.35$ was used for all σ_{absAE} .
- **Fig. S10**. Comparison of σ_{absAE} with (1) Weingartner and (2) Collaud Coen filter-loading corrections with σ_{absTAP} using all 5-min averages. A $C_f = 4.35$ was used for all σ_{absAE} . The solid line is 1:1.
- **Fig. S11.** Comparison of σ_{absAE} with Drinovec filter-loading correction and Schmid scattering correction using (1) Arnott parameters and (2) Collaud Coen parameters with σ_{absTAP} using all 5-min averages. A $C_f = 4.35$ was used for all σ_{absAE} . The solid line is 1:1.
- Fig. S12. Comparison of σ_{absAE} with Drinovec filter-loading correction plus Arnott scattering correction using (1) Arnott parameters and (2) Collaud Coen parameters with σ_{absTAP} using all 5-min averages. A $C_f = 4.35$ was used for all σ_{absAE} . The solid line is 1:1.

Figures

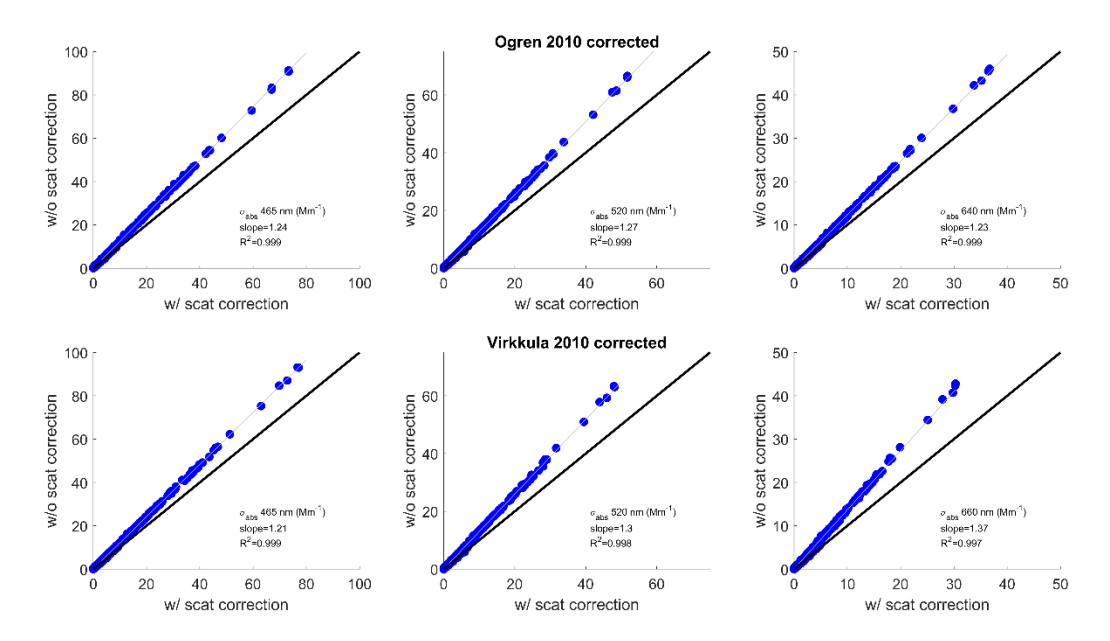


Fig. S1

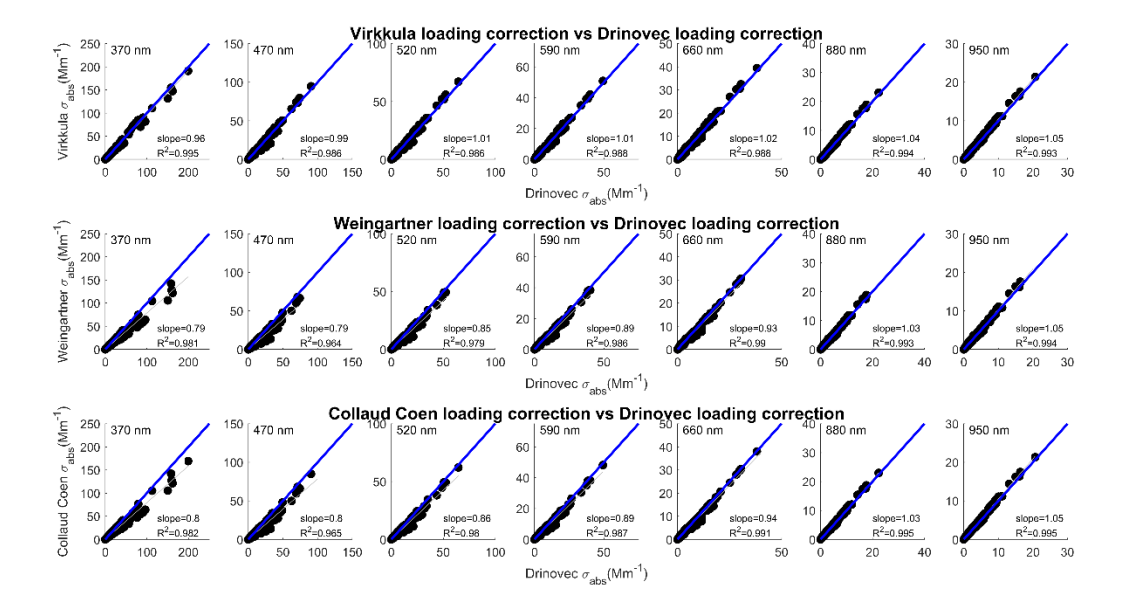


Fig. S2

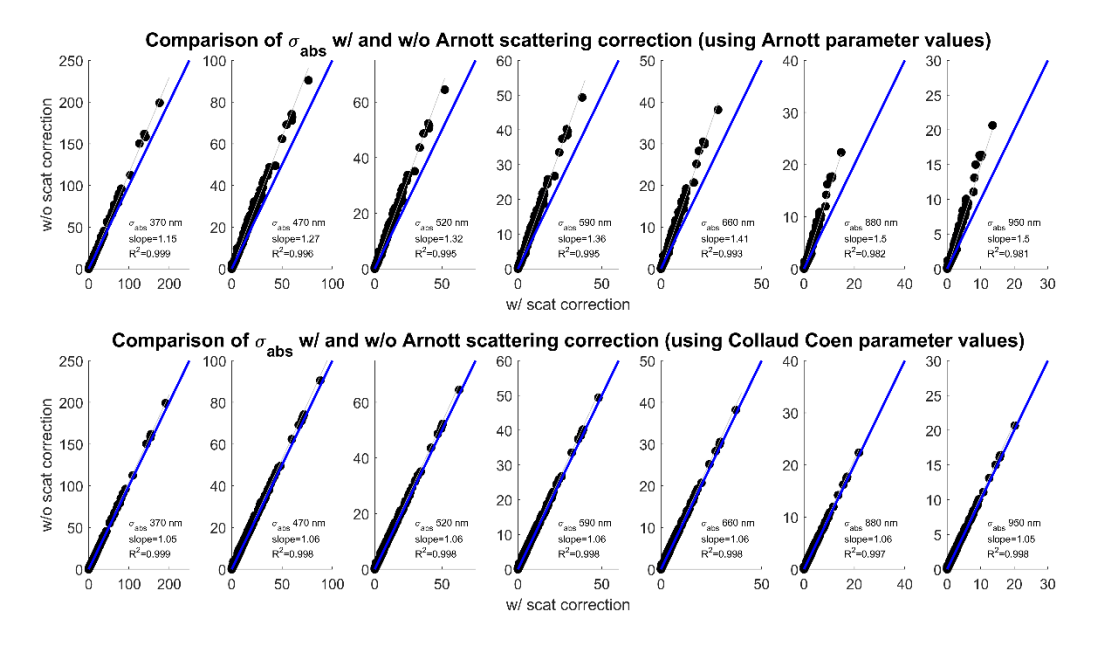


Fig. S3

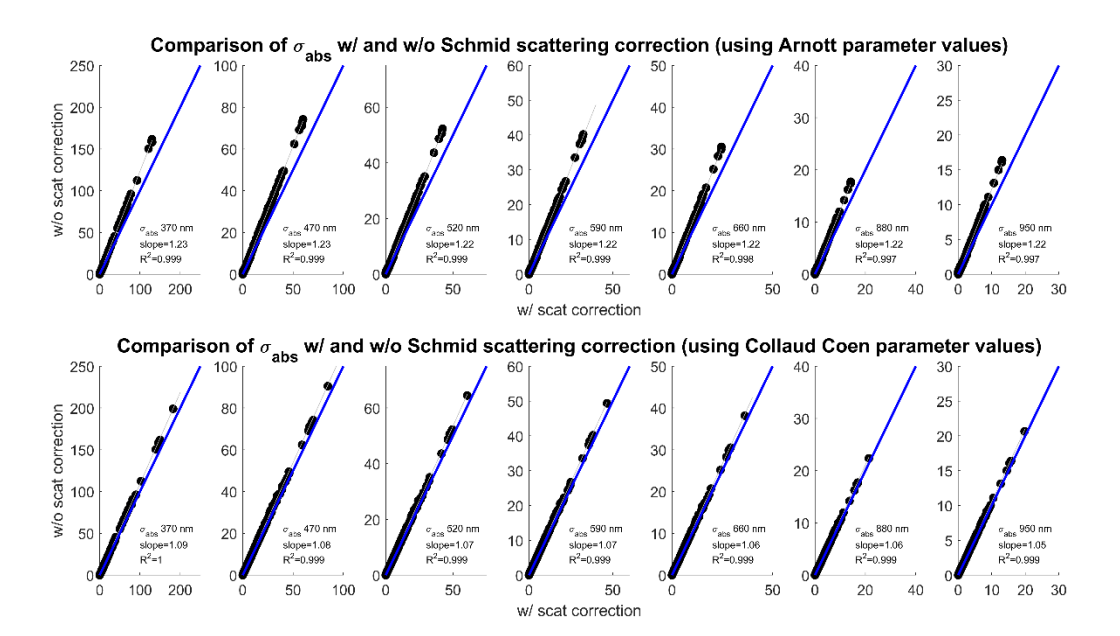


Fig. S4

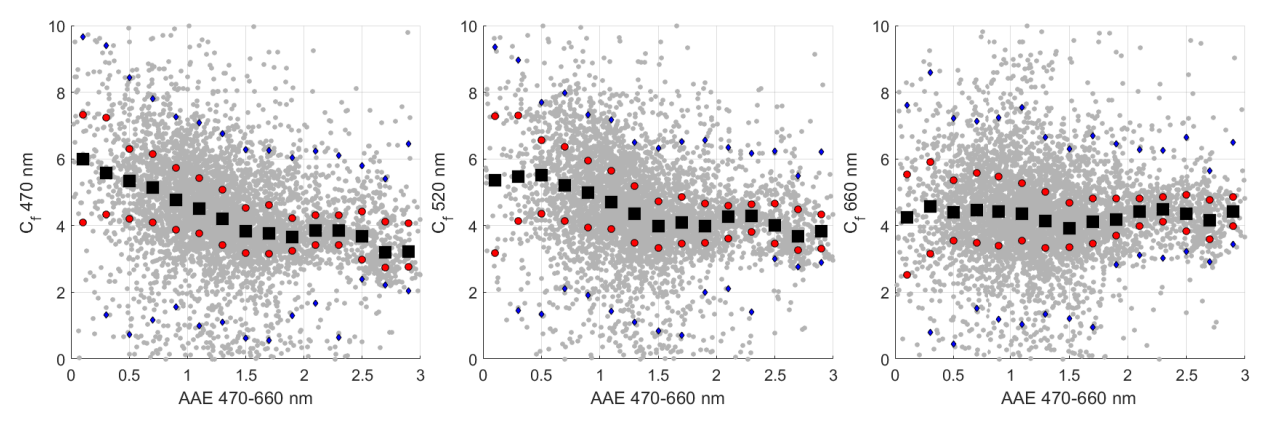


Fig. S5

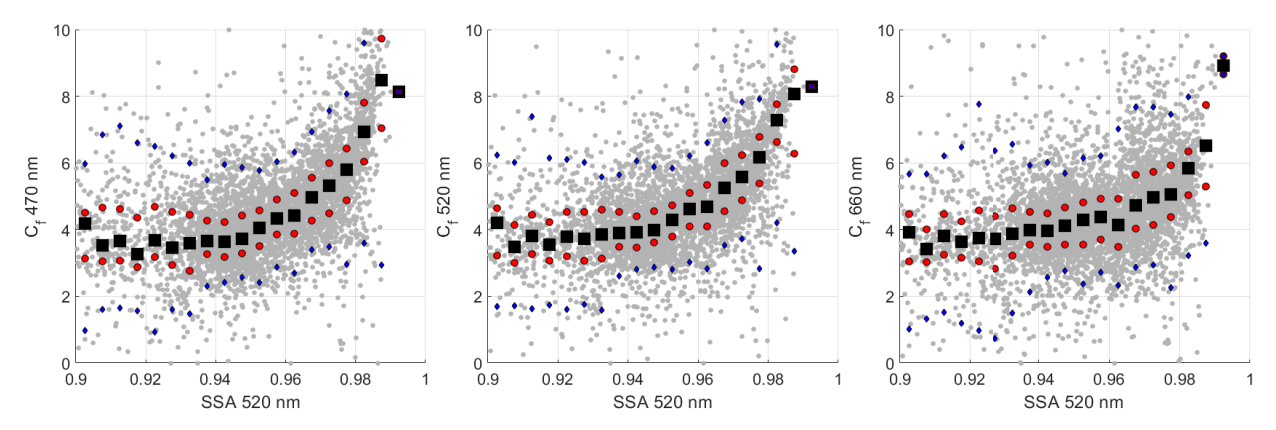


Fig. S6

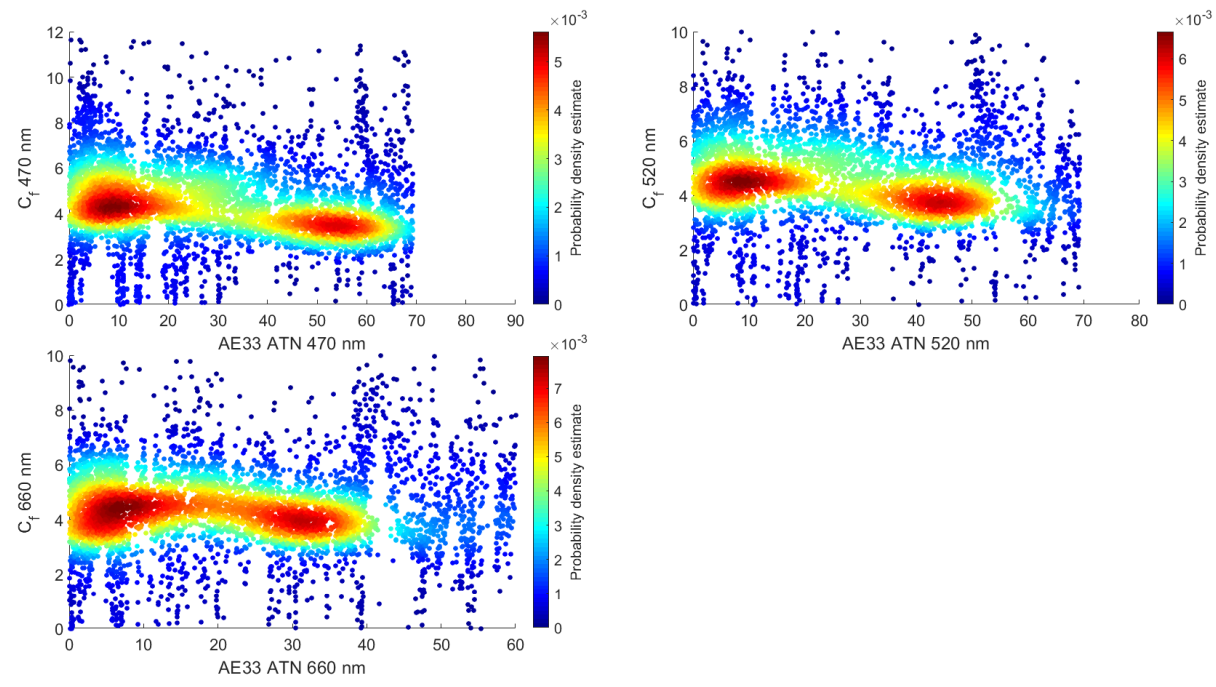


Fig. S7

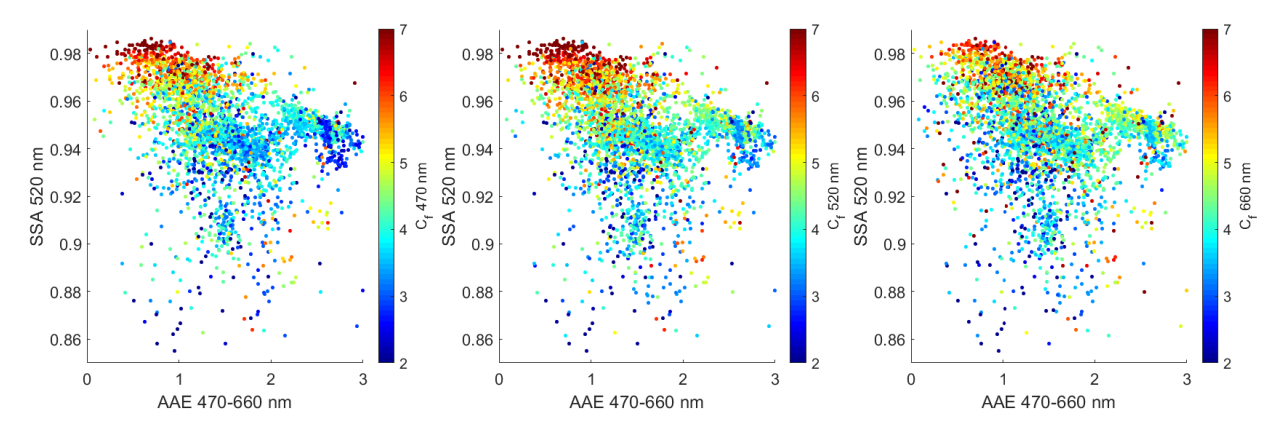


Fig. S8

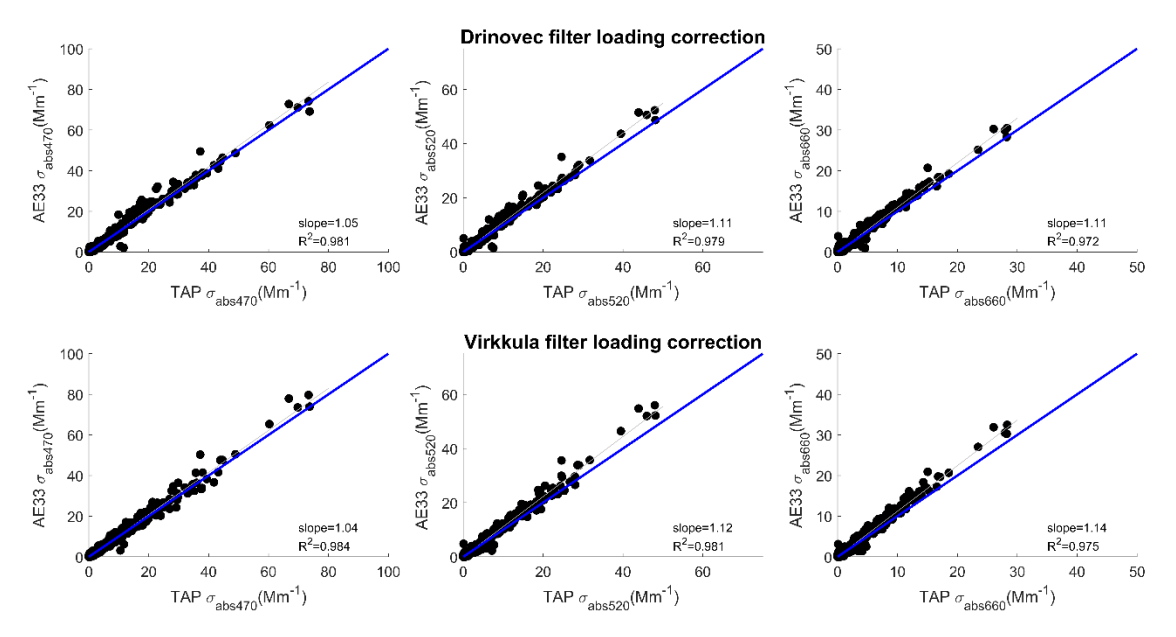


Fig. S9

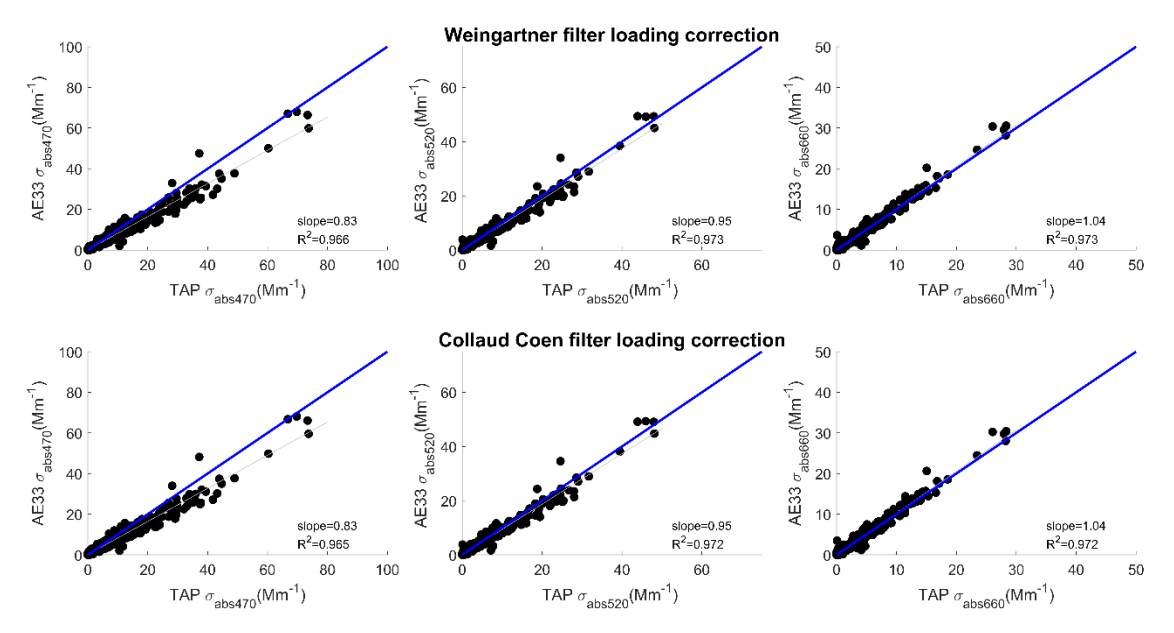


Fig. S10

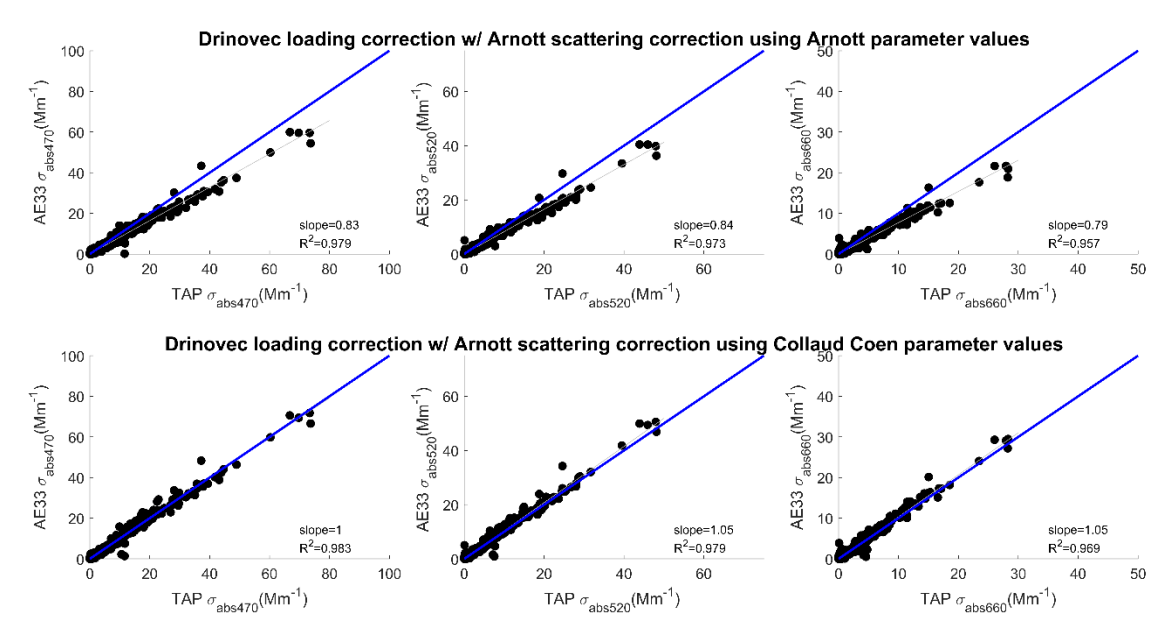


Fig. S11

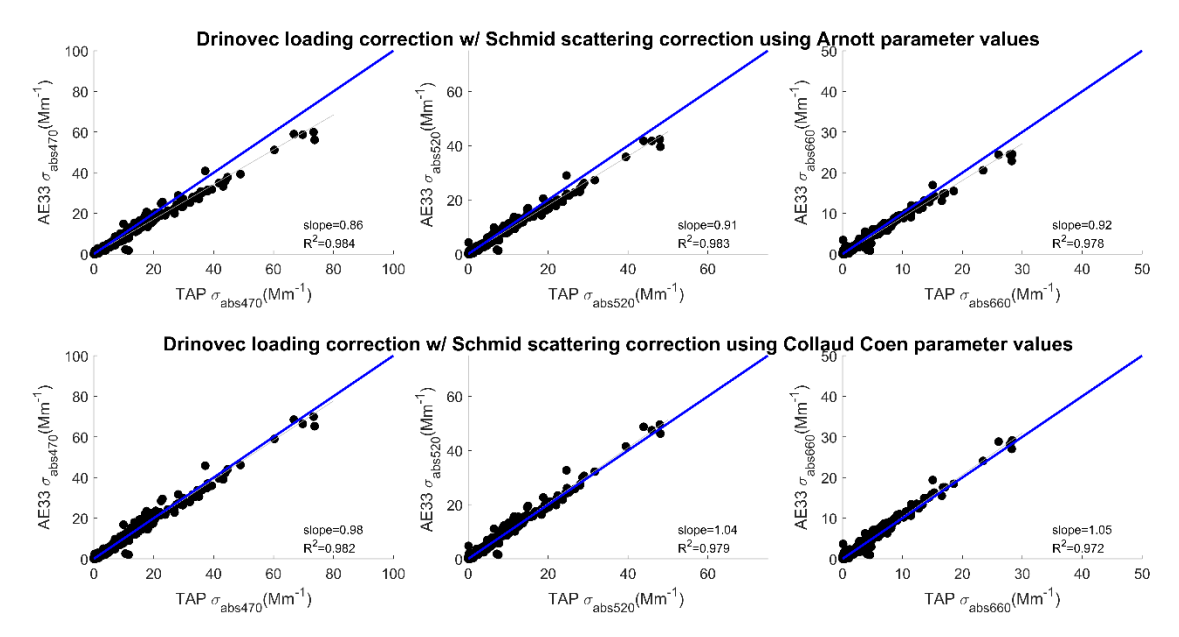


Fig. S12